

## Additional Evaluation of the Spatiotemporal Evolution of Rotation during Tornadoogenesis Using Rapid-Scan Mobile Radar Observations

JANA LESAK HOUSER,<sup>a</sup> HOWARD B. BLUESTEIN,<sup>b</sup> KYLE THIEM,<sup>b</sup> JEFFREY SNYDER,<sup>c</sup> DYLAN REIF,<sup>b</sup> AND ZACHARY WIENHOFF<sup>b</sup>

<sup>a</sup> *Department of Geography, The Ohio State University, Athens, Ohio*

<sup>b</sup> *School of Meteorology, University of Oklahoma, Norman, Oklahoma*

<sup>c</sup> *NOAA/OAR/National Severe Storms Laboratory, Norman, Oklahoma*

(Manuscript received 1 September 2021, in final form 22 March 2022)

**ABSTRACT:** This study builds upon recent rapid-scan radar observations of mesocyclonic tornadoogenesis in supercells by investigating the formation of seven tornadoes (four from a single cyclic supercell), most of which include samples at heights < 100 m above radar level. The spatiotemporal evolution of the tornadic vortex signatures (TVSs), maximum velocity differentials across the vortex couplet, and pseudovorticity are analyzed. In general, the tornadoes formed following a non-descending pattern of evolution, although one case was descending over time scales  $O(<60)$  s and the evolution of another case was dependent upon the criteria used to define a tornado, and may have been associated with a rapidly occurring top-down process. Thus, it was determined that the vertical sense of evolution of a tornado can be sensitive to the criteria employed to define a TVS. Furthermore, multiple instances were found in which TVSs terminated at heights below 1.5 km, although vertical sampling above this height was often limited.

**SIGNIFICANCE STATEMENT:** It is generally well understood that tornadoes form over short time scales [i.e.,  $O(\sim 60)$  s]. Despite this fact, detailed scientific measurements of tornado evolution during and just prior to genesis remains limited, particularly very near the ground and on time and space scales sufficient to observe tornado processes. Multiple recent studies have supported a non-descending evolution of rotation in supercell tornadoes, but the small number of analyzed cases is still insufficient for generalization. This study investigates seven new cases of tornadoogenesis using high spatiotemporal resolution radar data that include near-ground level observations to examine the evolution of rotation with time and height. For the time scales observable by the radar platform [i.e.,  $O(\sim 30)$  s], genesis occurred predominately following a non-descending manner in five out of the seven tornadoes studied, while the vertical evolution of two tornadoes were sensitive to the criterion used to define a “tornadic” vortex signature.

**KEYWORDS:** Atmosphere; Supercells; Tornadoes; Radars/Radar observations

### 1. Introduction

Tornadoogenesis and, particularly, the manner by which tornado-strength rotation makes contact with the ground have long been a topic of deep interest to the meteorological community. Several early idealized numerical simulations and

observational studies initially suggested that the evolution of strong vertical vorticity associated with tornado formation occurred in a rather slow [time scales  $O(\sim 5\text{--}10)$  min (Mitchell et al. 1998; Trapp 1999)], top-down manner by which the strong vorticity associated with the nascent tornado descended from storm midlevels to the ground (e.g., Leslie 1971; Smith and Leslie 1978, 1979; Burgess et al. 1975; Brown et al. 1978; Donaldson 1978). Leslie (1971) and Smith and Leslie (1978, 1979) attributed this evolution to the “dynamic pipe effect.” However, even during the same era, other numerical simulations and observational studies concluded that tornadoes could form following a non-descending pattern of evolution by either 1) developing nearly simultaneously over the depth of a rotating column in contact with the ground via convergence and amplification of vorticity (e.g., Rotunno 1977; Klemp and Rotunno 1983; Rotunno 1986; Wicker and Wilhelmson 1995), or 2) developing in a bottom-up manner from a region of strong but shallow [i.e.,  $O(100)$  m] near-ground vertical vorticity that is subsequently stretched and advected upward (e.g., Burgess and Donaldson 1979; Johnson et al. 1987; Brady and Szoke 1989; Wakimoto and Wilson 1989; Wilczak et al. 1992; Vasiloff 1993; Grasso and Cotton 1995; Roberts and Wilson 1995; Trapp and Mitchell 1995; Lee


---

Thiem’s current affiliation: National Weather Service, Peachtree City, Georgia.

---

Wienhoff’s current affiliation: Wind Engineering Research Laboratory, University of Illinois at Urbana–Champaign, Urbana, Illinois.

---

 Denotes content that is immediately available upon publication as open access.

---

 Supplemental information related to this paper is available at the Journals Online website: <https://doi.org/10.1175/MWR-D-21-0227.s1>.

---

*Corresponding author:* Jana Lesak Houser, [houserj@ohio.edu](mailto:houserj@ohio.edu)

DOI: 10.1175/MWR-D-21-0227.1

© 2022 American Meteorological Society. For information regarding reuse of this content and general copyright information, consult the [AMS Copyright Policy](#) ([www.ametsoc.org/PUBSReuseLicenses](http://www.ametsoc.org/PUBSReuseLicenses)).

and Wilhelmson 1997). The former process traditionally was discussed in the context of mesocyclonic tornadoes while the latter process was noted primarily in non-mesocyclonic tornadoes [i.e., land spouts (Bluestein 1985)], although there was also evidence to support a hybrid-type pattern where a mesocyclone merged with an area of low-level rotation generated outside the supercell (Wakimoto et al. 1998; Ziegler et al. 2001) just prior to tornadogenesis.

More recently, dynamic scale analysis (Bluestein et al. 2003) as well as visual and mobile radar observations from datasets having volume update times on the order of  $\sim 5\text{--}30$  s (e.g., Bluestein et al. 2010; Lee et al. 2012; French et al. 2013, 2014; Snyder and Bluestein 2014; Houser et al. 2015; Kurdzo et al. 2015; Kurdzo et al. 2017; Griffin et al. 2019; Wienhoff et al. 2020) ascertain that at least some tornadoes do indeed form and/or evolve very rapidly [i.e.,  $O(1\text{--}10)$  s], suggesting the original dynamic pipe effect hypothesis is likely not accurate, at least in the tornadoes examined. With the advent of high-resolution computer models (grid spacing  $< \sim 100$  m) (e.g., Wicker and Wilhelmson 1995; Bryan and Fritsch 2002; Xue et al. 2003; Mashiko et al. 2009) and rapid-scan radar ( $t < 30$  s between consecutive volume scans) (Wurman and Randall 2001; Bluestein et al. 2010; Pazmany et al. 2013; Isom et al. 2013), the details of tornadogenesis have been revisited with improved spatiotemporal resolution over the past decade. Results from such studies have *not* found evidence of a traditional [i.e.,  $O(5\text{--}10)$  min] DPE top-down evolution and have instead supported a non-descending<sup>1</sup> evolutionary process in supercells (e.g., Mashiko 2016; Mashiko et al. 2009; French et al. 2013; Kosiba et al. 2013; Dahl 2015; Dahl et al. 2014; Markowski and Richardson 2014; Naylor and Gilmore 2014; Xue et al. 2014; Houser et al. 2015; Parker and Dahl 2015; Schenkman et al. 2014; Markowski et al. 2018; Yokota et al. 2018; Bluestein et al. 2019; Wienhoff et al. 2020; Noda and Niino 2010). Moreover, French et al. (2013) determined that observations of tornadogenesis with insufficient temporal resolution (e.g., that of traditional WSR-88D observations) could be misidentified as having top-down evolution when they truly have non-descending evolution owing to the common presence of transient tornadic vortex signatures (TVSs) (Burgess et al. 1975; Brown et al. 1978; Brown and Wood 2012) at midlevels.

The above studies have helped to shift the tornadogenesis paradigm to favor non-descending evolution, at least for many tornadoes produced by supercells (which constitute most of the high-resolution radar-based analyses of observed tornadogenesis). However, to date, there remains a paucity of observational data sets that have both rapid volumetric temporal updates [i.e., volumetric retrieval  $O(<60)$  s] and near ground observations (i.e., heights  $< \sim 100$  m AGL). The

French et al. (2013), Houser et al. (2015), and Bluestein et al. (2019) studies analyze rapid-scan, volumetric observations of tornadogenesis occurring in a non-descending manner, but only four tornadoes were studied collectively. The Bluestein et al. (2019) study observed the evolution of TVSs below  $\sim 300$  m above radar level (ARL) but only one tornado was analyzed. Wienhoff et al. (2020) also provide an overview of multiple instances of tornadogenesis with near-ground data that occurred in a prolific tornado-producing supercell near Dodge City, Kansas. While they did not thoroughly examine the spatiotemporal evolution of the TVS, their analyses also suggest a non-descending pattern.

Numerical simulations of individual supercells from high-resolution models have been increasingly successful at resolving tornado-scale [ $O(100)$  m or less] rotation with fine near-ground vertical resolution (e.g., Mashiko et al. 2009; Dahl et al. 2014; Markowski and Richardson 2014; Orf et al. 2017; Yokota et al. 2018). These studies have also concluded that simulated tornado-like vortices often begin with strong near-ground rotation prior to the development of a vertically continuous vortex. They furthermore agree that the transition to a fully developed tornado is rapid and commonly occurs in a non-descending manner. However, computational and observational complications exist in resolving tornado flow near the ground (e.g., Marquis et al. 2008; Wurman et al. 2010; Murdzek et al. 2020; Wang et al. 2020). Additionally, despite the general consensus found within these recent modeling studies, near-ground observations are still required to confirm the models are appropriately representing real atmospheric conditions and produce results similar to observed events. Therefore, the evolution of near-ground rotation with time just prior to and during tornadogenesis remains an important topic that warrants additional observational study.

Herein, we present volumetric, rapid-scan radar observations of the time–height evolution of rotation based upon Doppler velocity measurements of TVSs during seven tornadogenesis events, most of which include observations within 100 m of the ground. Such data are critical to understanding the sequence of events occurring during tornado formation and to corroborating the results from numerically simulated tornado-like vortices.

## 2. Instrumentation and methodology

Radar data were acquired from the Rapid scan, X-band Polarimetric mobile radar platform (RaXPol) (Pazmany et al. 2013). RaXPol is capable of scanning a  $360^\circ$  plan-position indicator sequence in 2 s, which is accomplished by frequency hopping (Doviak and Zrnić 1993) and a high-speed pedestal. The horizontal and vertical (3 dB) beam widths are natively  $\sim 1^\circ$ , but the horizontal beamwidth is typically degraded to  $\sim 1.4^\circ$  during rapid-scan mode due to beam smearing. The range resolutions in the datasets collected herein vary from 15 to 75 m. Data are time stamped based upon an internal GPS-synchronized clock. Elevation angles for which data are collected in a volume are generally from  $0^\circ$  to  $20^\circ$  with  $2^\circ$  increments or  $0^\circ\text{--}10^\circ$  with  $1^\circ$  increments (Table 1). For additional

<sup>1</sup> In this study, we collectively refer to bottom-up and simultaneous intensification evolutionary modes as “non-descending” in order to be consistent with Trapp and Davies-Jones (1997), who first proposed two tornadogenesis modes (descending and non-descending). We also note here that this term is not truly representative of a process per se, but rather the temporal evolutionary mode.

TABLE 1. Summary of deployments for which tornadoes are analyzed in this study. Date is the local calendar date the data were collected. Deployment lat/lon is the latitude–longitude location for the radar deployment site. Location is the general area where the radar was deployed. Roll and pitch measure how off level of the platform was from side-to-side (roll) and front-to-back (pitch) in degrees. Radar (SPC 2020) genesis is the radar-based (SPC storm data recorded) tornadogenesis time. EF rating is the EF scale rating of the tornado based upon the SPC storm data report. El range is the range of elevations angles contained within the radar volume scan and Int is the elevation acquisition interval (in degrees). Height range (ARL) is the range of heights above radar level for which observations of the tornado were obtained over the duration for which data were analyzed. Dist to tor is the range of distances to the tornado and the area of interest over the analysis times. Vol scan time is the volume acquisition time, or the time it took to collect a full volume of radar data. On 27 May 2017, the first tornado (TV1), was ongoing at the time of deployment. As such, there is not a radar genesis time listed for this tornado. No other tornadoes (TV2–TV5) were reported in the official storm database on this date, despite visual and radar evidence to support their occurrence. Therefore, all other tornadoes are given an unofficial rating here as EFU.

Date	Deployment lat/lon	Location	Roll	Pitch	Radar genesis (UTC)	SPC genesis (UTC)	EF rating	El range and Int	Height range (ARL)	Dist to tor	Vol scan time
25 May 2012 Tor 1	38.69737°N, 98.95912°W	Russel County, KS	−0.19°	0.634°	~0142 (26 May)	0144 (26 May)	EF0	1°–17°, 2°	0.2–4.5 km	12–13 km	~26 s
25 May 2012 Tor 2	38.79830°N, 98.85456°W	Rush County, KS	0.18°	2.55°	~0237 (26 May)	0240 (26 May)	EF2	1°–17°, 2°	0.07–1.8 km	5 km	~26 s
27 May 2015	35.8888°N, 100.3982°W	E of Canadian, TX	0.25°	−0.12°	TV1: N/A	2305	EF3	0°–10°, 1°	0–1.5 km	~8 km	~28 s
27 May 2015	Same as above		0.25°	−0.12°	TV2: 2317	No report	EFU	0°–10°, 1°	0–1.5 km	~7 km	~28 s
27 May 2015	Same as above		0.25°	−0.12°	TV3: 2323	No report	EFU	0°–10°, 1°	0–1.5 km	~7 km	~28 s
27 May 2015	Same as above		0.25°	−0.12°	TV4: 2327	No report	EFU	0°–10°, 1°	0–1.5 km	~6 km	~28 s
27 May 2015	Same as above		0.25°	−0.12°	TV5: 2337	No report	EFU	0°–10°, 1°	0–1.5 km	~6 km	~28 s
22 May 2016	34.7004°N, 100.6122°W	Hall County, TX	0.18°	1.513°	~2351	2344	EF2	0°–20°, 2°	0–6 km	14–16 km	~28 s

details about the capabilities and technical specifications of RaXPol, the reader is referred to [Pazmany et al. \(2013\)](#).

After data acquisition and processing, the time–height evolution of the tornado-scale circulation being examined was determined by tracking spatiotemporally coherent RaXPol Doppler velocity couplets (regions of strong inbound and outbound velocities approximately azimuthally adjacent to each other) (e.g., [Fig. 1](#)). First, the radar-estimated time of tornadogenesis was determined by identifying when a nearly vertically continuous TVS (as subjectively determined by the authors) was present throughout the majority of the depth over which radar data were collected for cases with data domains terminating at or below 2 km ARL, or over at least the lowest 1.5 km in cases where deeper volume scans were collected. Following this, the maximum inbound and outbound velocity values within the tornadic or pre-tornadic velocity couplet were determined manually and were tracked backward with time for at least 5 min prior to the radar-specified tornadogenesis time, then forward 1–2 min. Similar to the methodology used in [French et al \(2013\)](#), [Houser et al. \(2015\)](#) and [Thiem \(2016\)](#), velocity couplet intensities and their corresponding latitude/longitude locations were quantified over all elevation angles according to (1), even if a TVS (as defined below) was not present at one or more elevation:

$$\Delta V_{\max} = \Delta V_{\max_{\text{outbound}}} + |\Delta V_{\max_{\text{inbound}}}|. \quad (1)$$

Note that, although inbound velocities are negative, we use  $V_{\max_{\text{inbound}}}$  to refer to the highest magnitude of the negative

inbound velocity. In cases where one or both maxima were not discernable, the approximate height at the location where a velocity couplet was expected based upon other elevation angles or upon the temporal continuity from scan to scan at that elevation angle was noted as well. This was done in order to document times and heights where velocity couplets were absent but may have appeared at later times or may have indicated vertical discontinuities in the TVS.

Developing consistent and quantitative criteria that defined a velocity couplet as a TVS proved to be a challenge. No formal definition of what constitutes a “tornadic” vortex exists, and the numeric threshold for defining a TVS based upon peer-reviewed literature varies from study to study, even when comparing mobile-radar based observations. For example, using WSR-88D imagery, the threshold is 11 m s<sup>−1</sup> of gate-to-gate shear ([Mitchell et al. 1998](#)), while [Alexander and Wurman \(2008\)](#), [Marquis et al. \(2012\)](#), and [Kosiba et al. \(2013\)](#), provide what is widely considered as the standard for mobile radar based tornadogenesis criteria, requiring a TVS to have a  $\Delta V_{\max}$  of at least 40 m s<sup>−1</sup> over a distance < 2 km since a 20 m s<sup>−1</sup> wind coupled with a 10 m s<sup>−1</sup> translation speed is sufficient for causing EF0 damage. However, [French et al \(2013\)](#) used a 25 m s<sup>−1</sup> threshold to compensate for a broad beam while [Houser et al \(2015\)](#) required a 50 m s<sup>−1</sup> velocity differential and [Wienhoff et al. \(2020\)](#) specified a 60 m s<sup>−1</sup> threshold because those  $\Delta V_{\max}$  values corresponded with the onset of damage as specified by NWS damage surveys. In the context of this study, a strict  $\Delta V_{\max}$  based definition of 40 m s<sup>−1</sup> over a distance < 2 km did not consistently

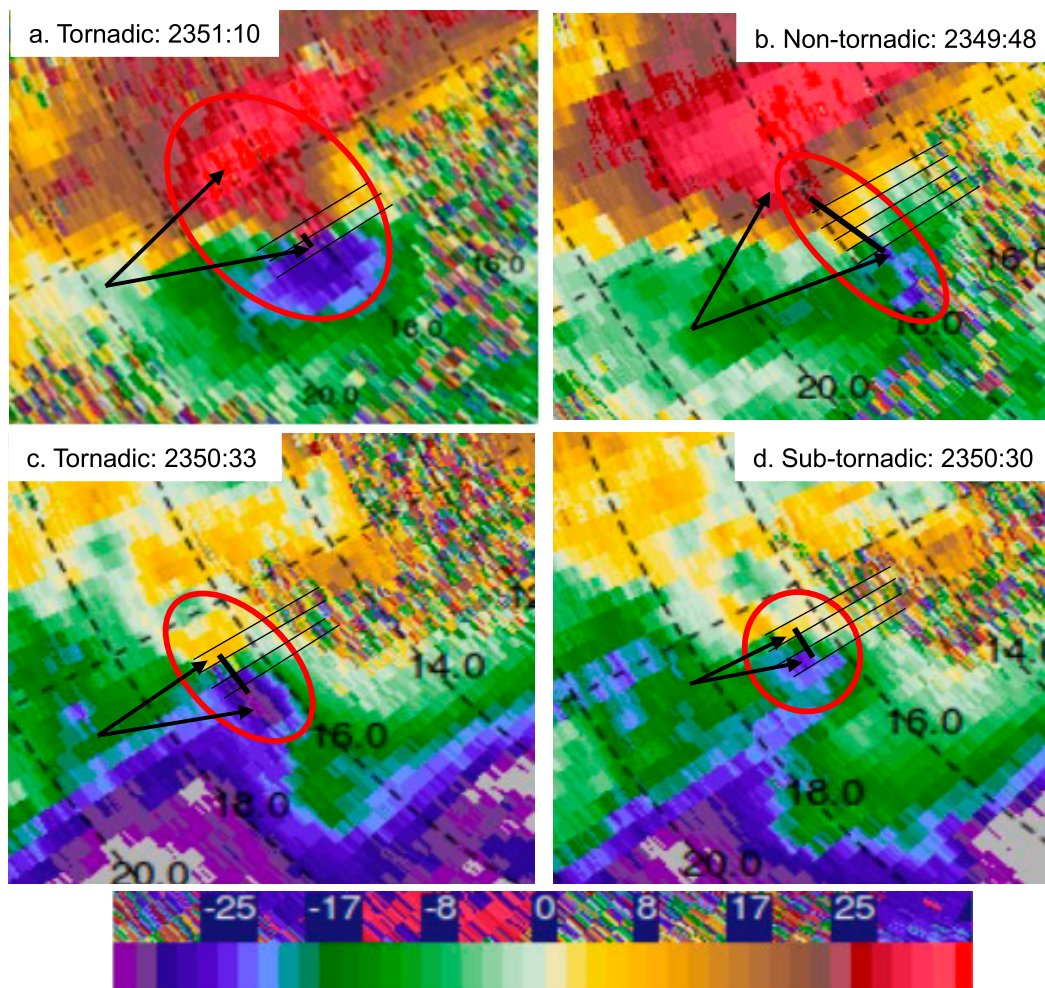


FIG. 1 Examples of various velocity couplets evident in the radial velocity field ( $\text{m s}^{-1}$ ) from 22 May 2016 and how they were classified. Arrows point to the maximum inbound and outbound velocities. Wide, short black lines show the distance where  $\Delta V > 40 \text{ m s}^{-1}$  is met. Thin black lines are azimuthal radials for ease of interpretation. (a) Tornadic velocity signature with  $\Delta V_{\text{max}}$  values that are  $>1 \text{ km}$  apart, but with the inner three radial  $\Delta V > 40 \text{ m s}^{-1}$  criteria met. (b) Non-tornadic velocity couplet with  $\Delta V_{\text{max}} > 40 \text{ m s}^{-1} < 2 \text{ km}$  apart, but inner three radial  $\Delta V > 40 \text{ m s}^{-1}$  criteria not met. (c) Tornadic velocity couplet with  $\Delta V_{\text{max}} > 40 \text{ m s}^{-1} < 1 \text{ km}$  apart. (d) Sub-tornadic velocity couplet with  $\Delta V_{\text{max}} < 40 \text{ m s}^{-1}$ , but  $>25 \text{ m s}^{-1}$  and a pseudovorticity  $> 0.1 \text{ s}^{-1}$ . Gray colors denote pixels where the velocities exceeded the range on the color bar (from  $-35$  to  $35 \text{ m s}^{-1}$ ).

agree with visual and damage survey evidence of tornadoes. In several cases, it was determined that there was visual evidence from the radar crew and/or time-stamped chaser videos of a tornado when  $\Delta V_{\text{max}}$  was as low as  $30 \text{ m s}^{-1}$ , while in other cases, velocity couplets having  $\Delta V_{\text{max}} > 40 \text{ m s}^{-1}$  with maxima separated by distances that met the  $<2 \text{ km}$  criterion were obviously larger than the tornado-scale rotation. The former discrepancy most likely occurred because the tornado was too small or too far away from the radar to be fully resolved, which negatively biased the magnitudes of the radial velocities since the smaller-scale extrema were not resolved by the radar (e.g., Brown et al. 1978; Brown and Wood 2012; French et al. 2013; Griffin et al. 2019). In the latter scenario, the tornadoes were also small and were weak, and/or shallow;

the larger diameter features were typically found above the TVSs and were more like narrow but intense low-level mesocyclones (e.g., Wienhoff et al. 2020).

Considering the inconsistency between cases when imposing a definition of a TVS based upon the value of  $\Delta V_{\text{max}}$ , pseudovorticity was employed to provide additional quantitative information about the vortices (Cai 2005) according to

$$\zeta_p = 2\Delta V_{\text{max}}/R. \quad (2)$$

Here,  $\Delta V_{\text{max}}$  is again the maximum velocity differential observed in the vortex, and  $R$  is the distance between the latitude/longitude points of these two observations, calculated using the

Haversine method (Inman 1835). Calculation of vertical vorticity using this method assumes a solid-body vortex that is axisymmetric about the vertical axis of rotation. While this assumption is idealized and typically does not truly represent real tornadoes, this method provided a consistent measure of tornado rotation strength from case to case. It is assumed that this parameter will sufficiently represent the intensity of a one-cell, single vortex tornado, even when the storm-motion vector positively biases the side of the vortex parallel to the storm motion vector, because the opposite side experiences a comparable negative bias such that the velocity differential across the TVS ultimately remains the same. Consequently, the cases examined herein have a structure that suggests they are one-celled vortex tornadoes, for which we maintain that this metric will provide a reasonable estimate of intensity. However, we do note that a full 3D wind synthesis was not performed and therefore, we cannot rule out a two-celled structure, in which case the pseudovorticity may not accurately represent the intensity of the tornado.

Because of the uncertainty in quantifying a “tornadic” TVS, we have opted to compute four different criteria for tornadic and sub-tornadic strength TVSs, as follows. Criteria 1a and 1b were developed in tandem, based upon a subjective comparison of what the authors considered TVSs, and they were combined in the final analysis of TVSs under the auspices of criterion “1.”

**Criterion 1a:**  $\Delta V_{\max} > 40 \text{ m s}^{-1}$  with  $< 2 \text{ km}$  between maxima as long as there were no more than three adjacent azimuthal radials<sup>2</sup> separating inbound and outbound velocities having  $\Delta V \geq 40 \text{ m s}^{-1}$  (e.g., Figs. 1a,b) (there could be more than three radials separating the maxima in  $\Delta V$ ). This criterion enabled large tornadoes to be included, but differentiated between those with tight azimuthal velocity gradients (Fig. 1a), which were presumably tornadic, from those which still met the  $\Delta V > 40 \text{ m s}^{-1}$  over  $< 2 \text{ km}$  criterion, but had a weaker azimuthal velocity gradient and were obviously not tornadic (Fig. 1b).

**Criterion 1b:**  $\zeta_p$  that was  $> 0.1 \text{ s}^{-1}$ , as long as  $\Delta V > 30 \text{ m s}^{-1}$ . This criterion enabled a narrow vortex that did not meet the  $40 \text{ m s}^{-1}$  criterion to be considered a tornado as long as its  $\Delta V$  was at least  $30 \text{ m s}^{-1}$  and  $\zeta_p$  was strong enough (Fig. 1c).

A sub-tornadic vortex designation was also included in the analyses to identify trends associated with strengthening velocity couplets transitioning from the sub-tornadic to tornadic

threshold (or vice versa). A velocity couplet was considered sub-tornadic if (i)  $25 \text{ m s}^{-1} < \Delta V < 30 \text{ m s}^{-1}$  and  $\zeta_p > 0.1 \text{ s}^{-1}$  (Fig. 1d), or (ii)  $30 \text{ m s}^{-1} < \Delta V < 40 \text{ m s}^{-1}$  and  $0.08 \text{ s}^{-1} < \zeta_p < 0.1 \text{ s}^{-1}$ . Criterion i was implemented because it met the  $\zeta_p$  criteria of a tornado, but the  $\Delta V$  values were too low. We decided on  $25 \text{ m s}^{-1}$  as the lower limit because values lower than this included a variety of vortices that were never related to tornadoes. Criterion ii was implemented to include situations where the  $\Delta V_{\max}$  values were potentially within tornadic range, but the distance may have slightly exceeded the three-radial condition, bringing the pseudovorticity value down.

**Criterion 2:**  $\Delta V > 30 \text{ m s}^{-1}$  over a distance  $< 1 \text{ km}$  regardless of the pseudovorticity value, with a sub-tornadic threshold of  $25 \text{ m s}^{-1} < \Delta V < 30 \text{ m s}^{-1}$ . This criterion appeared to agree well with the onset of tornado formation based upon photographic evidence for tornadoes having a small radius of maximum wind, but it likely included sub-tornadic vortices for 22 May 2016, which had a larger radius of maximum wind than the other cases.

**Criterion 3:**  $\zeta_p > 0.1 \text{ s}^{-1}$  as long as  $\Delta V > 20 \text{ m s}^{-1}$ , with a sub-tornadic threshold of  $0.8 < \zeta_p < 0.1 \text{ s}^{-1}$ . This criterion was used to specifically investigate the issue of how low-biased velocity values for far-range tornadoes might be impacted by changing the criteria. It also appeared to agree well for the small tornadoes with the onset of tornadogenesis from visual evidence, but it did not work for the 22 May 2016 case, as the distance between the maxima was large, which consistently reduced  $\zeta_p$  values below  $0.8 \text{ m s}^{-1}$  even when the tornado was known to be occurring.

### 3. Data

For this study, data were obtained from five RaXPol deployments on three days and include analysis of tornadogenesis in seven tornadoes (Table 1; Fig. 2). Two tornadoes (rated EF0 and EF2) occurred in central Kansas on 25 May 2012 (Figs. 3a,b). Four weak, shallow, short-lived tornadoes [one rated EF2, the rest were not recorded in the SPC ONETOR database (SPC 2020; Schaefer and Edwards 1999)] were observed in a cyclic supercell on 27 May 2015 in the northeastern Texas Panhandle (Figs. 3c,d). The final tornado (EF2) was from 22 May 2016 in the southeastern Texas Panhandle, southwest of Memphis, Texas (Fig. 3e).

There was some ambiguity regarding whether all of the vortices analyzed from the 27 May 2015 dataset were truly tornadoes, as three were not associated with official tornado reports, and they were shallow, relatively weak, and occurred over open land where minimal, if any, damage could be detected. However, based upon the quantitative criteria established for this study and since three out of the four vortices<sup>3</sup> were clearly associated with a tornadic debris signature [TDS, e.g., Ryzhkov et al. (2005); Bluestein et al. (2007); Kumjian and Ryzhkov (2008)],

<sup>2</sup> The criterion of three radials is subjective, and the physical distance between the three radials varied with the tornadoes' distances from the radar. However, we found this metric to be ideal when comparing it to our subjective identification of what made a couplet a TVS. A large, well-resolved tornado could hypothetically have more than three radials separating the  $40 \text{ m s}^{-1}$   $\Delta V$ . However, the tornadoes observed in this study were generally small, having diameters on the order of a few hundred meters and were typically observed from 5 to 15 km away (i.e. not at ultra-close range). The largest tornado (the 22 May 2016 tornado) had a distance between  $V_{\max_{\text{inbound}}}$  and  $V_{\max_{\text{outbound}}}$ , which periodically exceeded 1 km, but was also the farthest away from the radar. Thus, this criterion happened to still be suitable for this tornado.

<sup>3</sup> The low-level correlation coefficient data were compromised due to the presence of ground clutter for the second of the four tornadoes analyzed on this day (TV3), which made it impossible to determine if there was a TDS.

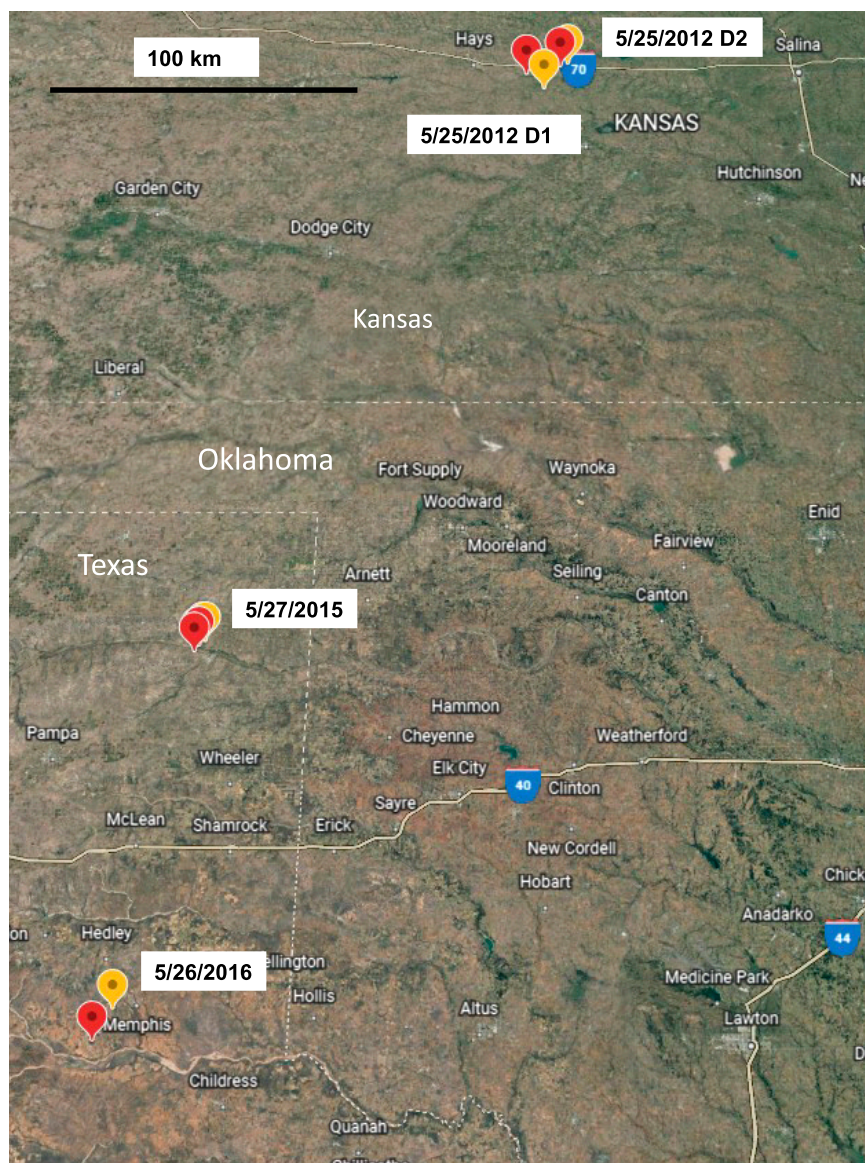


FIG. 2. RaXPOL deployment locations (yellow balloons) and tornado locations (red balloons) for the cases used in this study. There are four deployments from three days. D1 (D2) on 25 May 2012 is for tornado 1 (tornado 2). Tornado locations were determined from the TVS location at the time of tornadogenesis.

the vortices analyzed from this day were defined herein as tornadoes. Furthermore, there were storm chaser videos and photographs of multiple tornadoes, often becoming rain-wrapped, that occurred during the deployment timeframe. Unfortunately, many of these videos and photographs did not have timestamps that were sufficiently accurate to be used for formal comparisons in the results/analysis of this study. Since multiple tornadoes formed over short time frames, it was not possible for us to know for certain which photographs/videos were associated with which radar-indicated tornado. Nevertheless, these chaser resources provide evidence that at least some, if not all, of the vortices analyzed were indeed tornadoes, despite the absence of formal storm reports.

No aspect-ratio correction<sup>4</sup> was applied to the radial velocity data to estimate the impacts of under-sampling the tornadic wind fields—we have opted to keep the analysis to the

<sup>4</sup> A draft of the “Estimating Wind Speeds in Tornadoes” standard from the American Society of Civil Engineers recommends an aspect ratio correction following:  $1.0/[1.0 - 0.24 \times (2.0BW/X_D)]$ , where BW is the radar beam width in degrees, and  $X_D$  is the angular distance between maximum velocity observations in the radar data (J. Snyder 2021, personal communication). The aspect ratio correction is capped at 8.6% (equivalent to having seven radials in the diameter of maximum winds) since correction factors can become very large for very poorly sampled tornadoes.



FIG. 3. Photographs of several of the tornadoes studied herein. Tornado 1 from (a) 0142 and (b) 0143 UTC 25 May 2012 southwest of Russell, KS. Tornado 2 on this day occurred after dark. TV1 and TV5 from (c) 2306 and (d) 2339 UTC 27 May 2015 from Canadian County, TX. (e) The tornado at 2352 UTC 22 May 2016. Photographs (a),(b) courtesy of Jana Houser. Photographs (c) and (d) courtesy of Jeff Snyder. Photograph (e) courtesy of Alec Scholten.

measured data instead of trying to compensate for sampling errors. Additionally, corrections for the non-zero pitch and roll of the radar (Table 1) were not made. A hydraulic leveling system was used for the deployments, but the instrument was still not perfectly leveled, which introduces errors when estimating the physical location of the radar observation. However, the offsets in all datasets were generally  $<1^\circ$  and, while such errors could be important in a quantitative sense or if we were performing additional computations such as dual-Doppler syntheses or trajectory analyses, they will not meaningfully impact the overall analysis of the TVS intensity or  $\Delta V_{\max}$  trends.

During two of the deployments (six tornadoes), RaXPol collected data at the nominal  $0^\circ$  elevation angle (Table 1). There was some ground clutter contamination, but  $\rho_{\text{hv}}$  values

that were consistently in the meteorological scatterer range ( $>0.9$ ) suggested strong enough contribution from hydrometeors to permit the inclusion of velocity data from this elevation angle for most times. However, the observed magnitudes of these near-ground velocities are likely negatively biased due to the zero velocity contribution of the ground to the Doppler velocity estimates. No attempt was made to remediate this effect. The 27 May 2015 case suffered the most from beam blockage with the TVS at certain times being completely obscured by ground clutter. However, the overall interpretation of whether or not TVS behavior was descending or non-descending was not sensitive to the magnitude of the winds at this lowest height.

All heights of observations referenced are given as above radar level (ARL). While there will be some error in the

vertical placement of these measurements with respect to the physical height of the observations above *ground* level (AGL), the terrain is relatively flat in the regions where data were collected and errors will be on the order of tens of m. Furthermore, this limitation will not affect the trends of TVS characteristics with height, and the margin for error is less than the vertical beam width. Thus, we consider differences between ARL vs. AGL to be negligible in our examination.

We report that the velocity couplets from the  $0^\circ$  elevation angle are at a height of 0 m even though this is not precisely true, as the hydrometeor contribution to the signal is coming from the top  $\sim 1/2$  of the radar beam just above the surface, yielding a power-weighted centerline closer to  $0.2^\circ$ – $0.3^\circ$  in elevation (Snyder and Ryzhkov 2015). Considering the distance to the areas of interest which ranged from  $\sim 6$  to  $\sim 15$  km and the  $1^\circ$  vertical half-power beam width, the observations from the  $0^\circ$  elevation angle come from heights between the ground and  $< \sim 52$ – $130$  m ARL (i.e., the area within the nominal 3-dB beamwidth above the ground). The highest elevation angle at which data collection occurred was  $20^\circ$ . There likely will be some negative bias in the upper elevation angle Doppler velocity retrievals as a result of incompletely resolving the horizontal wind component (and increasingly sampling the vertical component). This bias affected the 22 May 2016 case most. If one considers a TVS that has a  $40 \text{ m s}^{-1} \Delta V_{\max}$  corresponding to a max  $V_{\text{in}} = -20 \text{ m s}^{-1}$  and a max  $V_{\text{out}} = +20 \text{ m s}^{-1}$ , the reduction in horizontal inbound/outbound velocity max values would be  $1.7 \text{ m s}^{-1}$  per side, or  $3.4 \text{ m s}^{-1}$  across the velocity couplet. This reduction is much less than the difference between low-level velocity differentials versus higher ones. Other datasets are affected even less. Thus, while the magnitude may be reduced aloft, it is not likely to affect the interpretation of the results.

The limitations described above affected the recorded Doppler velocity estimates and height specifications on a case-by-case basis, and the effects were inconsistent among cases. However, for this research, we were less interested in the specific values of the Doppler velocities and were instead interested in the spatiotemporal *trends* in velocities. The time periods and distance changes over which individual tornadoes were analyzed were short enough to neglect variations in Doppler velocity estimates over the analysis timeframe with the exception, perhaps, of the 27 May 2015 case. However, for that case, the distance to the storm's area of interest remained nearly constant, only varying by  $\sim 2$  km. Thus, despite some quantitative limitations associated with assessing the exact magnitude and location of Doppler velocities, it is clear that these cases nonetheless enabled us to analyze fine spatiotemporal resolution observations of tornadogenesis within  $\sim 50$ – $100$  m of the ground. For this reason, we are comfortable proceeding with our analysis.

#### 4. Observational results

##### a. 25 May 2012

###### 1) TORNADO 1

The supercell that produced the first tornado analyzed here developed between 2200 and 2300 UTC 25 May 2012 near Hays, Kansas, along a warm front. Mobile radar observations

commenced at 0137 UTC 26 May. During the 5 min preceding tornadogenesis, rotation at low levels ( $\sim 200$  m ARL) was generally weak, although a shallow velocity couplet was evident (Figs. 4a,c,e,g,i). The couplet was not apparent at heights  $\sim 1.5$  km (not shown), but above this, a stronger area of rotation was found aloft, slightly to the west of the lower-level couplet. This couplet was evident through the top of the sampling volume ( $\sim 3$  km; Figs. 4b,d,f,h,j). Despite the generally weak rotation, a TVS developed suddenly at multiple elevation angles throughout the vertical domain. Radar-estimated tornadogenesis time was between 0142 and 0143 UTC, when near-ground rotation was stronger and there was a nearly vertically coherent, narrow, contracted TVS through 3.5 km (Fig. 5).

Around 0137 UTC ( $\sim 5$  min prior to tornadogenesis), all TVS criteria indicated that the rotation above 2.5 km was strong enough to be considered tornadic. This rotation persisted nearly continuously until tornadogenesis, with the exception of about 1 min between 0141 and 0142 UTC, just prior to tornadogenesis (Figs. 4 and 6a–c). In contrast to what was happening aloft, but in agreement with the raw Doppler velocity images in Fig. 4, only weak rotation that periodically intensified to sub-tornadic strength (i.e.,  $\Delta V_{\max} > 25 \text{ m s}^{-1}$ ) was present, although  $\zeta_p$  did exceed  $0.1 \text{ s}^{-1}$  occasionally (Fig. 6c). The evolution of  $\Delta V_{\max}$  told a similar story to the TVS criteria as  $\Delta V_{\max}$  was consistently strongest aloft and was relatively weak at the lowest elevation angles (Fig. 7a). At  $\sim 0142$  UTC, there was a vertically continuous vortex from  $\sim 150$  m ARL through 3 km. The magnitude of rotation below about 1.5 km was considered sub-tornadic by criteria 1 and 2, but the pseudovorticity was tornadic. Based upon criteria 1a/1b and 2, the TVS appeared to descend rapidly between  $\sim 0141:30$  and 0143 UTC from a height of 3 km ARL to the surface (Figs. 6a,b). This descent occurred much faster than the hypothetical time scale of the dynamic pipe effect, implying that it could be occurring as the result of some non-DPE process over a much smaller time scale.

However, according to the  $\zeta_p$  TVS criterion, the TVS developed from the ground up. Thus, the sense of vertical evolution changed based upon what criterion is used to define a TVS. This complicates the interpretation of this case. It is important to note that the  $\Delta V_{\max}$  was  $< 40 \text{ m s}^{-1}$  at the  $1^\circ$  and  $3^\circ$  elevation angles ( $z \sim 200$ – $600$  m ARL) over a majority of the tornado's life cycle. Yet, despite the weak radar-observed velocities, visual evidence clearly indicates that a tornado was occurring (Fig. 3b). This is an example of the scenario given in section 2 in which the radar was relatively far from the tornado ( $\sim 15$  km), and the tornado was small. Consequently, the flow field in the tornado was not resolved well, resulting in an underestimation of the maximum wind speeds. It is therefore quite possible that some velocity couplets designated by  $\Delta V_{\max}$  criteria 1 and 2 as being sub-tornadic were actually tornadic. When examining the evolution of the numeric values of  $\Delta V_{\max}$  around this time (Fig. 7a), there is no evidence of intensification via the top-down process at the time of and just before tornadogenesis, although this does occur after tornadogenesis,  $\sim 0143$  UTC.

The quantitative values of  $\zeta_p$  (i.e., not the TVS criteria) support nearly simultaneous development of strong  $\zeta_p$  over

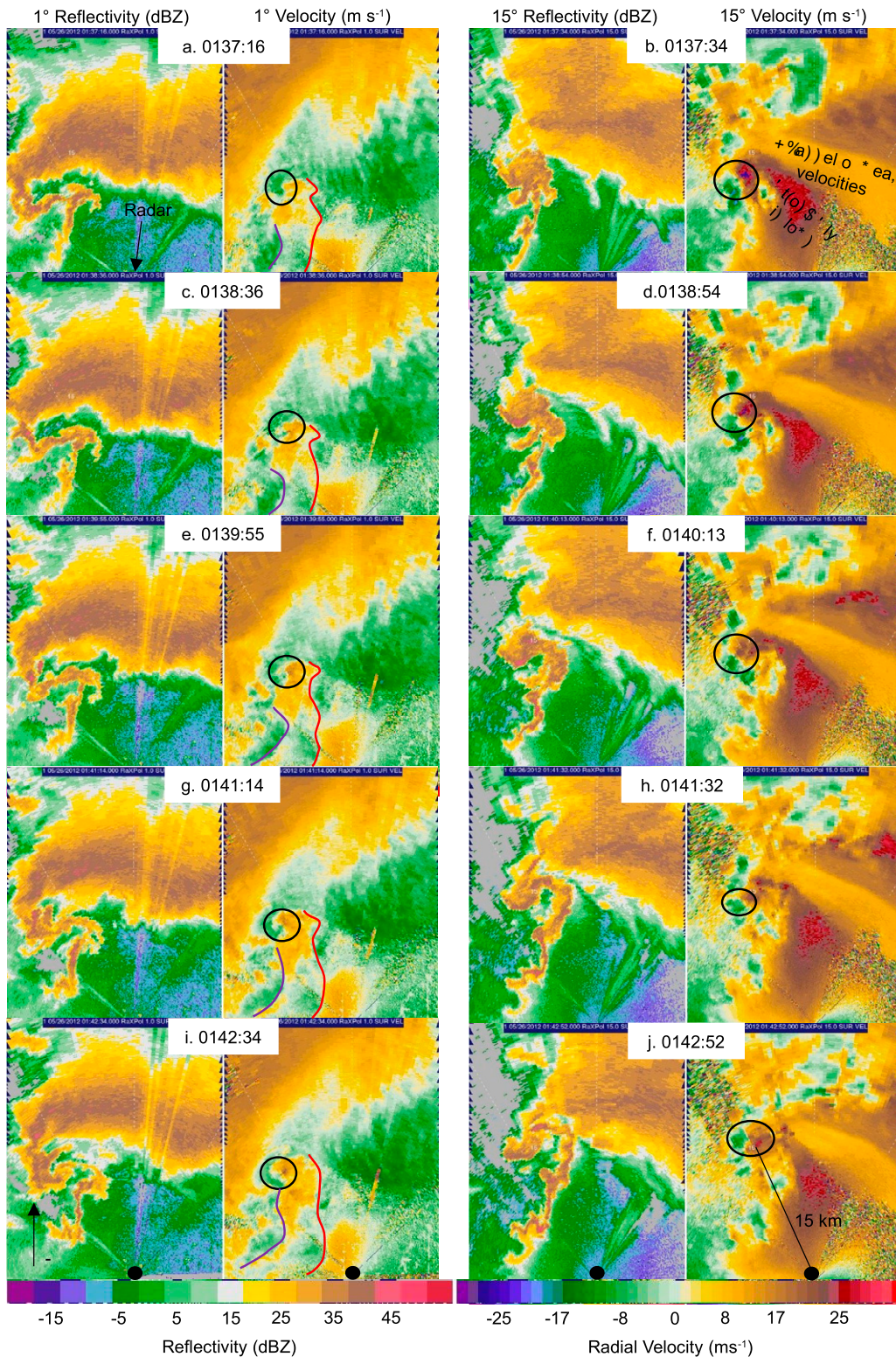


FIG. 4. (a)–(j) Evolution of the 25 May 2012 storm leading up to genesis of tornado 1 on this date (which occurred around 0142 UTC). Reflectivity (dBZ) at 1°, radial velocity ( $\text{m s}^{-1}$ ) at 1°, reflectivity (dBZ) at 15°, and radial velocity ( $\text{m s}^{-1}$ ) at 15°, shown in columns from left to right. Times are indicated for each scan next to the panel letter (UTC). The radar is located at the black dot as shown in (i) and (j). Panels above (i) and (j) were cropped so that the radar location is not shown. Heights of TVSs range from  $\sim 200$  to 220 m (3.5–3.8 km) ARL for the 1° (15°) observations.

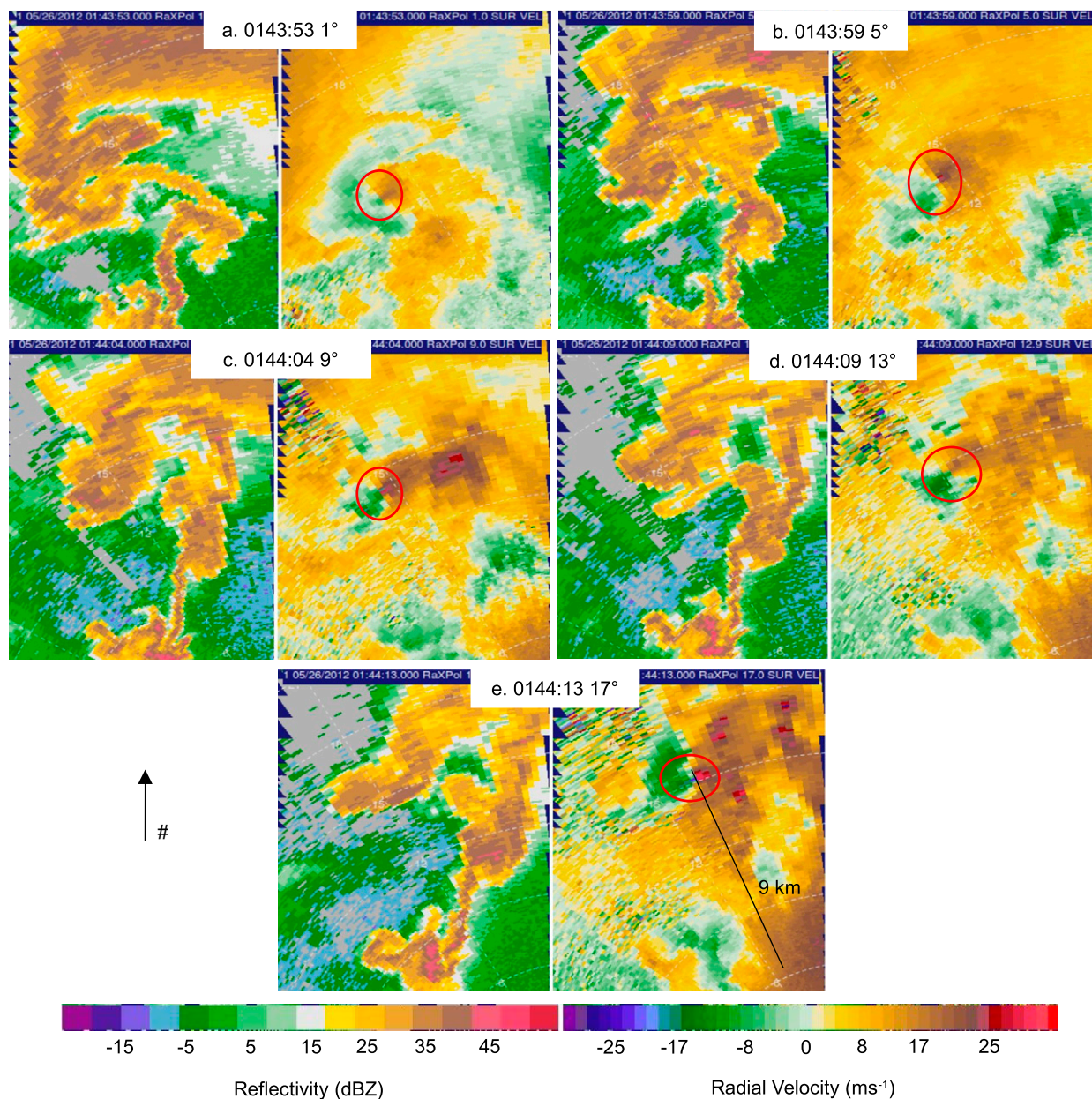


FIG. 5. (left) Reflectivity (dBZ) and (right) radial velocity ( $\text{m s}^{-1}$ ) images from select elevation angles for the volume scan at the time of tornadogenesis in tornado 1 of 25 May 2012. (a) 1° (~225 m), (b) 5° (1.2 km), (c) 9° (2.2 km), (d) 13° (3.3 km), and (e) 17° (4.4 km). Range rings are provided every 3 km. Red circles identify the TVS. All heights given are ARL at the approximate center of the vortex.

the lowest 2 km (Fig. 8a), except over the lowest 500 m where there is an indication of non-descending rotation between 0142 and 0143 UTC. Because  $\zeta_p$  is a function of both  $\Delta V_{\max}$  (which was rather weak and only minimally increased except at the lowest elevation angles) and the distance between maxima, the sudden intensification of  $\zeta_p$  over the lowest 2 km implies that the rotation simultaneously contracted at 0142 UTC (or it evolved faster than the temporal resolution of the radar), just prior to the development of the deep, continuous TVS noted around 0143 UTC in Fig. 6a. However, the shallow

layer of top-down evolution in the lowest 500 m suggests additional convergence may have been needed to intensify the weak near-ground rotation to tornadic intensity, or that a process facilitating downward advection of the stronger rotation above was needed.

It should be noted that  $\zeta_p$  is sensitive to errors in both  $\Delta V_{\max}$  and the distance between maxima. Thus, these results should be interpreted with some caution. However, since  $\zeta_p$  strengthened at the same time as the sudden onset of vertically continuous sub-tornadic TVS development evident in

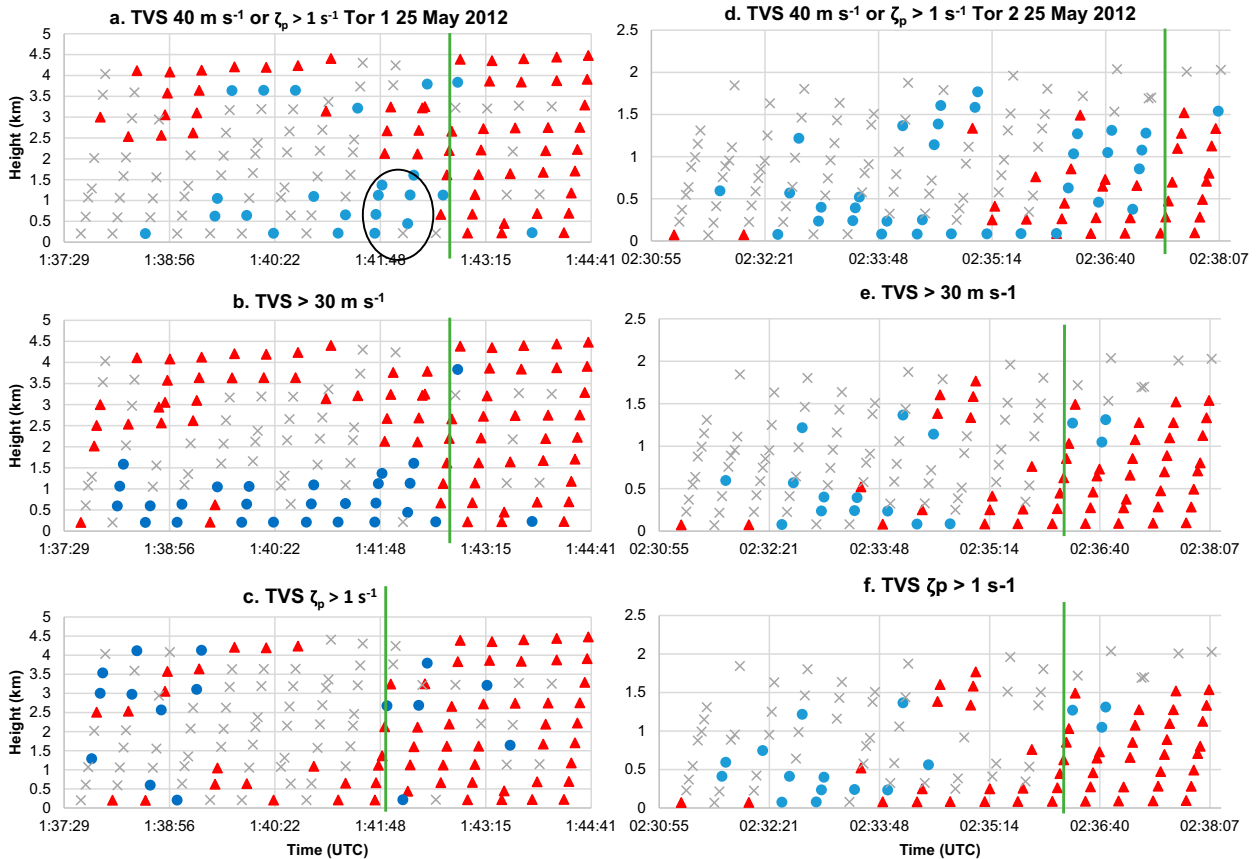


FIG. 6. Evolution of the TVSs (red triangles), sub-tornadic vortex signatures (filled blue circles), and locations where a vortex was absent (gray X marks) with time (x axis) and height (y axis) for all tornadogenesis cases using the three different tornadogenesis criteria described in section 2 (a)–(c) Case 1: tornado 1, 25 May 2012. (d)–(f) Case 2: tornado 2, 25 May 2012. For all cases, the top panel represents the results using criterion 1a/1b; the middle panel is for criterion 2; and the bottom panel depicts criterion 3. Green lines indicate times of radar-determined tornadogenesis. The quantitative designation of tornadic vs sub-tornadic criteria is given in section 2. Note that the axes are NOT the same scale in each figure panel. Images have been scaled according to physical print size.

Figs. 6a–c, we believe this result is not an artifact. The sudden intensification of  $\zeta_p$  supports the hypothesis that the TVS may indeed have been tornadic when  $\zeta_p$  exceeded the  $0.1 \text{ s}^{-1}$  threshold despite  $\Delta V_{\max}$  remaining  $< 30 \text{ m s}^{-1}$ . If these weaker TVSs designated as sub-tornadic using criteria 1 and 2 were actually tornadic, then the TVS would have developed nearly simultaneously over the lowest 3 km adjacent to the ground and the evolution of this tornado would be non-descending. *This discrepancy in interpretation illustrates the sensitivity of genesis evolution mode using the  $\Delta V_{\max}$  criteria, especially when analyzing a small TVS at relatively large distances (here  $\sim 15 \text{ km}$ ).*

In summary, tornado 1 was associated with a broad mid-level velocity couplet that was consistently stronger than the near-ground rotation. The tornado itself may have formed via a rapid (non-DPE) top-down process or from the nearly simultaneous convergence of low-level rotation over the lowest 2 km, or some combination of the two. This uncertainty is a result of ambiguous near-ground velocity estimates that were low-biased due to under-sampling of the small tornado. It is unclear if the sub-tornadic TVSs at low levels would have had

$\Delta V_{\max} > 35 \text{ m s}^{-1}$  if the vortex had been sampled at a shorter range from the radar (i.e., more fully sampled in space).

## 2) TORNADO 2

The same supercell that produced tornado 1 moved slowly northeastward, and RaXPOL was deployed again but at a closer range of only 5 km from the hook echo. Even though the same scanning strategy was used for this deployment as the previous one (Table 1), the geometry made the scanning volume shallower in the vertical at the area of interest; observations were recorded from  $\sim 70 \text{ m ARL}$  to just over 2 km ARL. Fine-scale vertical profiles of this tornado were also analyzed by Kosiba and Wurman (2013) at times later than the analyses herein.

Between 6 and 7 min prior to tornadogenesis (which occurred between 0236 and 0237 UTC based upon the different TVS criteria imposed in Figs. 5d–f), a well-defined, organized low-level mesocyclone and hook echo, with flanking precipitation again extending from the hook to the west and southwest was observed in the  $1^\circ$  elevation angle ( $\sim 70 \text{ m ARL}$ ) data (Fig. 9a).

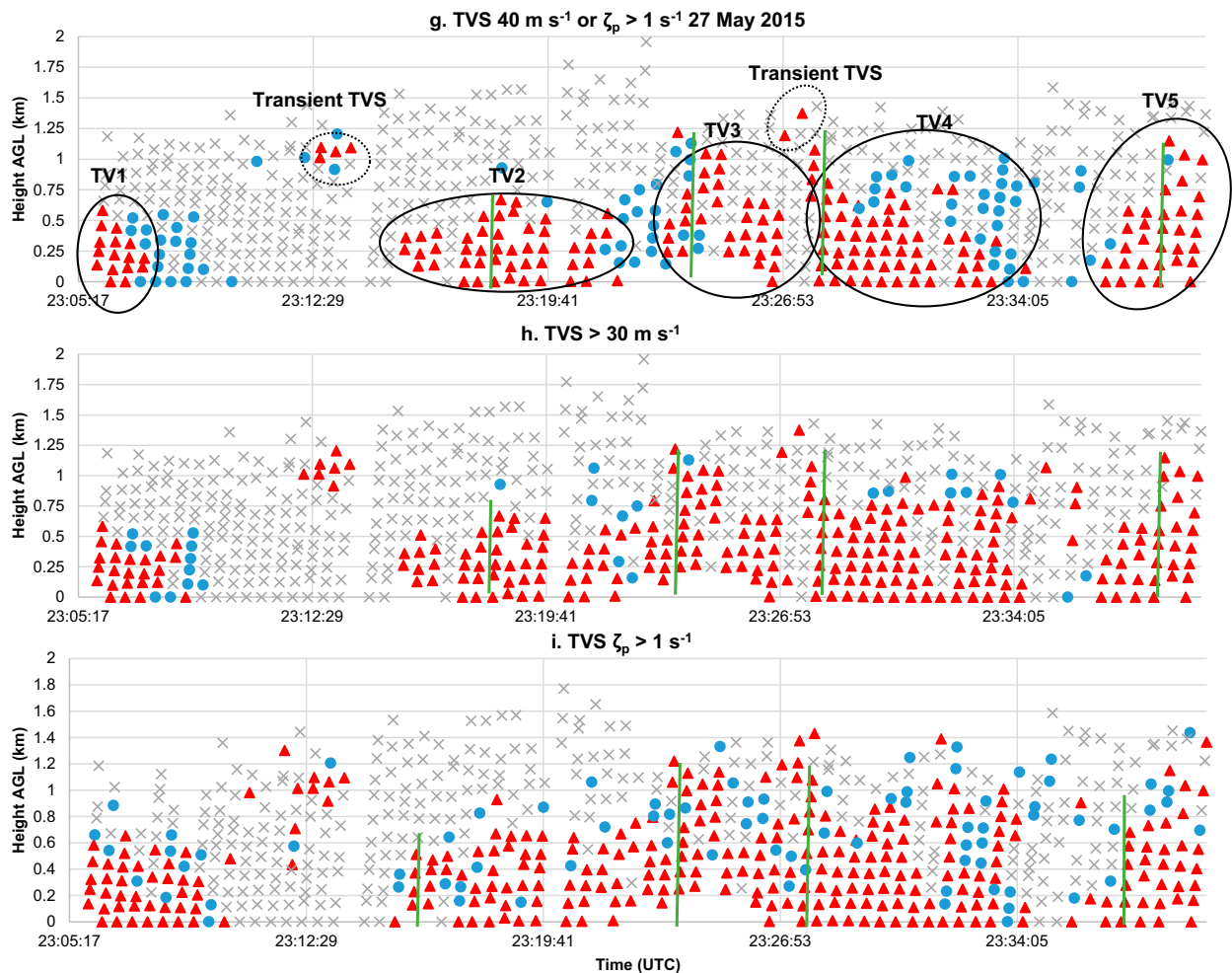


FIG. 6. (g)–(i) As in (a)–(c), but for cases 3–6: 27 May 2015.

Higher up, at  $17^\circ$  ( $\sim 1.3 \text{ km}$  ARL at the hook), the low-level mesocyclone was still apparent, but the flow was more turbulent, with small-scale pockets of weak velocities embedded within the flow on the inbound side of the mesocyclone (Fig. 9b).

Leading up to tornadogenesis, the hook appeared to “unwind” rather than curl up, in contrast to what is commonly found (Figs. 9a,c,e,g,i) (e.g., Bluestein et al. 2003; Tanamachi et al. 2012; Tanamachi et al. 2013). The low-level mesocyclone remained intact and rather unchanged in the  $1^\circ$  elevation angle observations ( $z \sim 100 \text{ m}$  ARL), although velocities near the nascent tornado strengthened and contracted while those farther away weakened slightly. However, in the  $17^\circ$  elevation angle data ( $z \sim 1.2 \text{ km}$  ARL), a band of outbound velocities appears in the center of the inbounds, causing the low-level mesocyclone to break apart and become disorganized (Figs. 9d,f,h,j).

Unlike what occurred with the earlier tornado on this day, there was persistent low-level and near-ground rotation that periodically achieved tornadic strength at heights  $< 500 \text{ m}$  for  $\sim 4 \text{ min}$  prior to the development of a vertically coherent vortex, and intermittently before that. Generally, the TVS

appears to have developed in a bottom-up manner, at least in the lowest  $2 \text{ km}$  over which data were collected (Figs. 6d–f). However, over the lowest  $500 \text{ m}$ , there is a slight discrepancy, with criterion 1a/1b indicating a top-down evolution of tornado-strength TVSs (Fig. 6d), while criteria 2 and 3 clearly argue a bottom-up evolution (Figs. 6e,f). However, the general pattern still appears to be bottom up. According to the  $\zeta_p$  criterion, a TVS existed at the lowest elevation angle ( $z \sim 10 \text{ s}$  of  $\text{m}$  ARL) for nearly  $2 \text{ min}$  prior to the upward development of strong rotation. This signal was also present in the other 2 TVS criteria, but was considered sub-tornadic for most times. There was no signal of a TVS descending from above the  $2\text{-km}$  vertical sampling domain and building downward with time, although there was a transient spin up to tornadic intensity at  $1.5 \text{ km}$  at 0234 UTC, about  $2 \text{ min}$  prior to genesis. It is entirely possible that tornadic-strength rotation may have existed somewhere above this height, but there was no TVS in the  $17^\circ$  elevation angle data ( $z \sim 2 \text{ km}$ ) until 0239 UTC, about  $2 \text{ min}$  after tornadogenesis occurred at lower heights (Fig. 10). Unfortunately, due to the lack of data collected above  $2 \text{ km}$ , it is unclear whether this height represents the

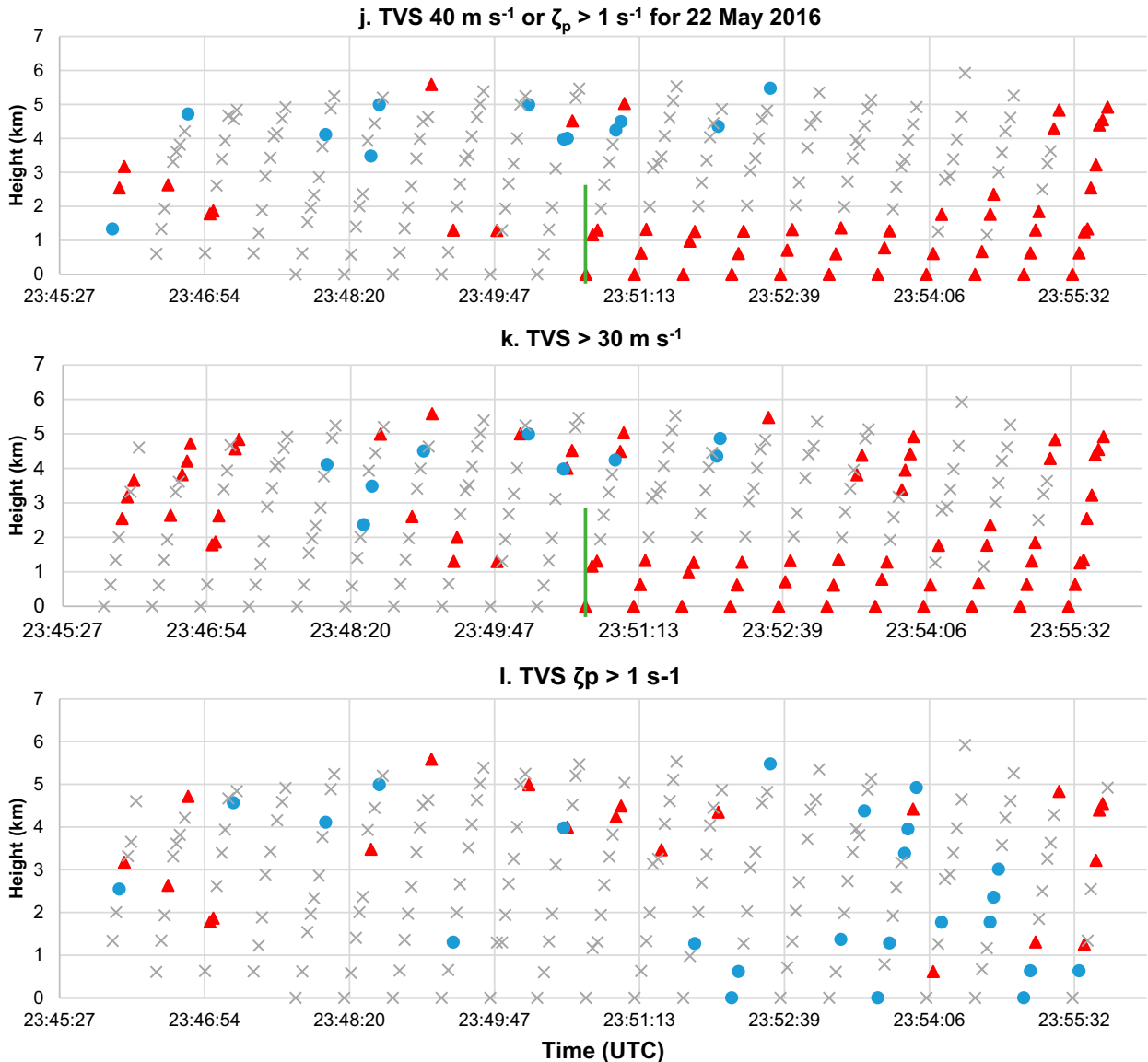


FIG. 6. (j)–(l) As in (a)–(c), but for case 7: 22 May 2016.

true vertical terminus of the tornadic circulation,<sup>5</sup> if it was an example where the rotation was weak in the vicinity of an inversion (French et al. 2014; Houser et al. 2015; Bluestein et al. 2019; Wienhoff et al. 2020), or if it appeared to be weakened because the vortex was highly tilted at this level (Bluestein 2022). No sounding data were available nearby, so it was not possible to confirm the environmental thermodynamic profile.

<sup>5</sup> In this case as well as the other cases where the vertical sampling domain was shallow, an attempt was made to cross reference WSR-88D data to confirm or refute the presence of TVSs at higher heights. However, due to the coarse spatial and temporal resolution of the WSR-88D imagery, this did not aid our interpretation of tornado structure. Furthermore, TVSs were often identified in the 88D imagery at times we knew there was no tornado.

When examining the trend in all values of  $\Delta V_{\max}$  (Fig. 7b), marginally tornadic rotation (it did not meet the spatial criterion to be considered a TVS because there was too much distance between the  $40 \text{ m s}^{-1}$  velocity differential) appeared to be advected downward from  $\sim 1 \text{ km}$  to  $\sim 400 \text{ m}$  prior to tornadogenesis ( $\sim 0232$ – $0235 \text{ UTC}$ ). It did not exhibit the characteristics of evolution associated with the dynamic pipe effect because strong rotation at the higher heights was not maintained over time, but it may represent forcing associated with some other top-down process. Ultimately, however, this descending region of stronger  $\Delta V_{\max}$  was not directly linked to the formation of the tornado as the  $\Delta V_{\max}$  values subsequently weakened prior to tornadogenesis. However, this process does appear to have strengthened the near-ground rotation and may have indirectly aided in tornadogenesis by providing near-surface vorticity rich air. At 0236 UTC,

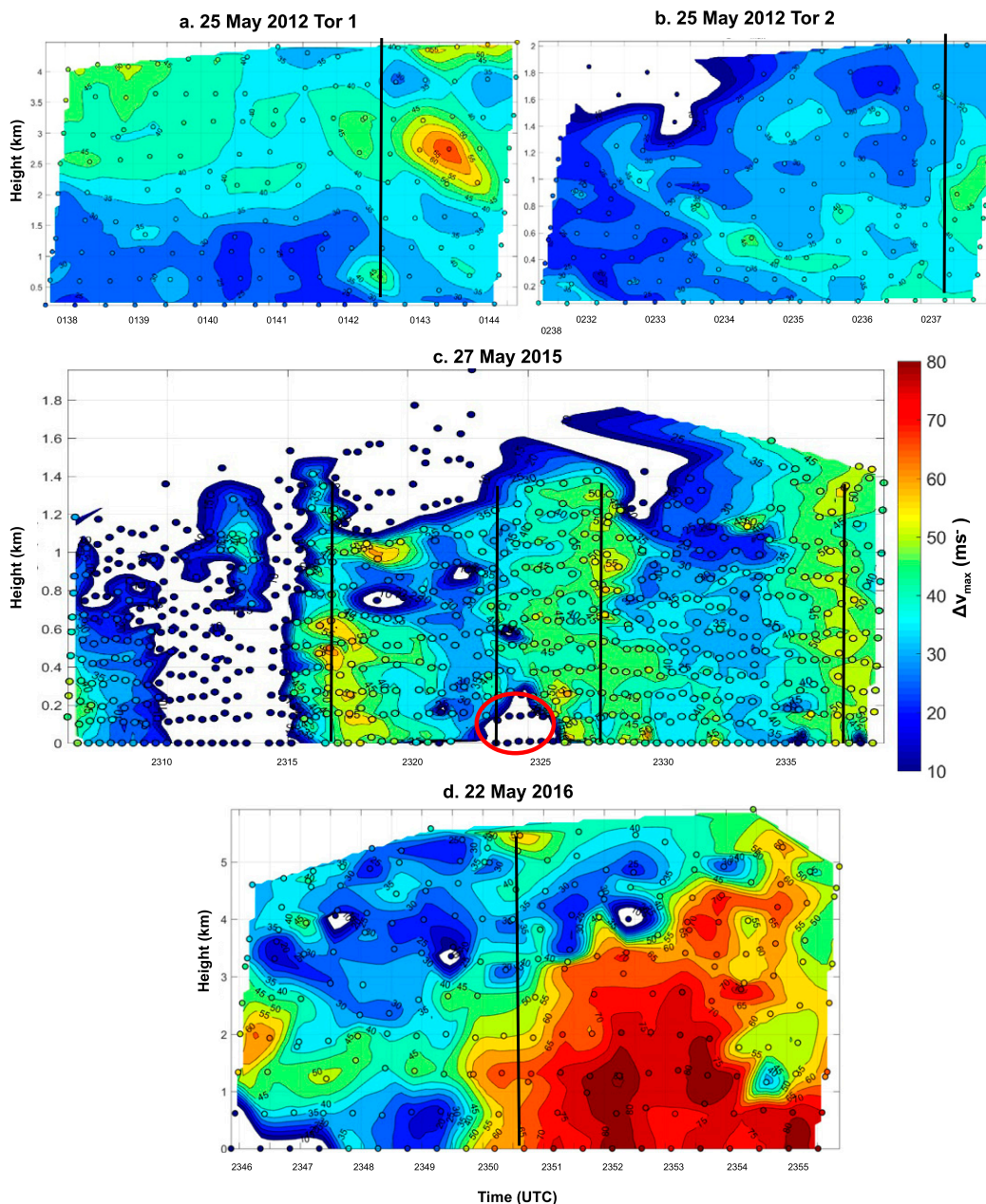


FIG. 7. (a)–(d) Evolution of  $\Delta V_{\max}$  (color shading;  $\text{m s}^{-1}$ ) with time ( $x$  axis; UTC) and height ( $y$  axis; km) for all five cases. The red circle in (c) indicates a region where ground clutter at the lowest 2–3 elevation angles created low-biased velocities. A velocity couplet was evident during these times, but its magnitude was substantially lower than those at higher elevations and later times in the tornado's life, when it moved outside of the contaminated area.

which was right around tornadogenesis time, the strongest  $\Delta V_{\max}$  values were located near the ground and weakened with height. After tornadogenesis, the velocities around 1 km ARL intensified and exceeded what they were at the lowest levels.

Similar trends are noted in the evolution of  $\zeta_p$  (Fig. 8b). However, the descending rotation between 0231 and 0235 UTC seen in  $\Delta V_{\max}$  is less obvious. Instead, the strongest  $\zeta_p$  was consistently near the ground, except for a few localized, transient maxima at other heights, and it built upward with

height between ~0235 and 0237 UTC. After tornadogenesis, rapid intensification occurred ~0238 UTC at nearly all heights below ~1.5 km, with the exception of the very lowest heights, which actually saw  $\zeta_p$  weaken briefly. We speculate that this sequence of events is suggestive of a bottom-up genesis process, followed by subsequent convergence and stretching as the tornado underwent initial intensification.

In summary, tornado 2 on 25 May 2012 likely formed from the bottom-up, although the vertical extent to the domain

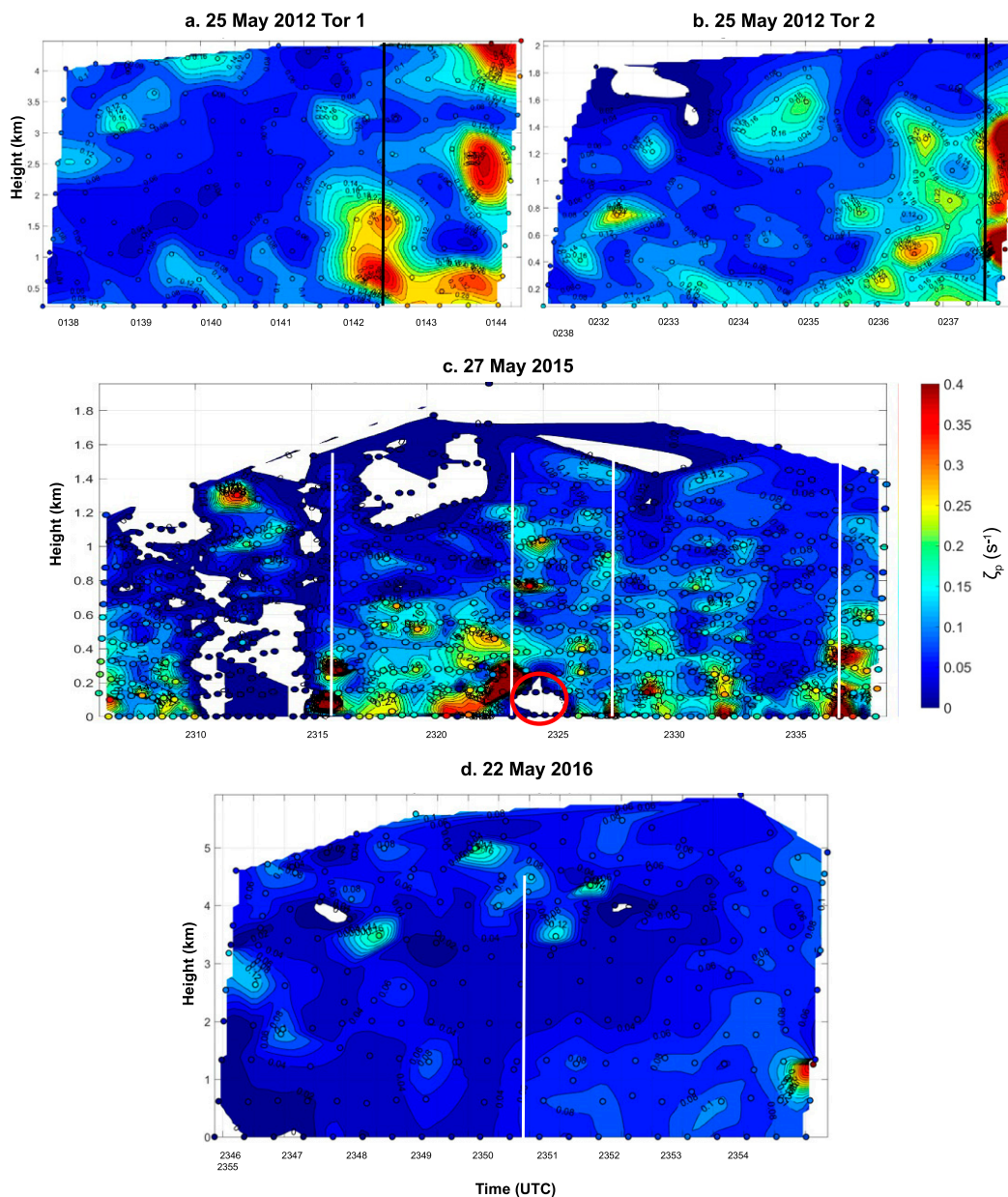


FIG. 8. As in Fig. 7, but for pseudovorticity (color contours;  $\text{s}^{-1}$ ). Solid vertical lines again indicate times of radar-determined tornadogenesis. No smoothing or filtering was applied to the  $\zeta_p$  field.

precludes the ability to analyze trends in rotation above 2 km. Strong rotation very near the ground was present throughout the 5–6 min prior to tornadogenesis. The TVS was initially confined to heights  $< 500$  m for about 1 min prior to the development of a deeper, coherent vortex, although the TVS terminated at a height of  $\sim 1.5$ –2 km where the low-level mesocyclone became disorganized above which, data were unavailable.

#### b. 27 May 2015

On 27 May 2015, RaXPOL commenced data collection at 2305 UTC on a cyclic supercell near Canadian, Texas, that had produced a relatively long-lived, nearly stationary

tornado at 2158 UTC [SPC ONETOR; SPC 2020; Griffin et al. (2019)]. At the onset of data acquisition, the aforementioned tornado had dissipated and the area of interest was about 6.5 km away. For this deployment, the data were concentrated at low heights ( $< \sim 1.5$  km ARL at the area of interest/tornado, Table 1). About 35 min of data were analyzed for this storm (rather than 8–10 min as in the other cases examined in this study) because there was persistent, tornado-strength rotation near and below 500 m for the majority of this time, which was associated with five tornadoes produced by the cycling mesocyclone (Figs. 6g,h,i and 7c). Individual mesocyclones often moved from east to west or southwest

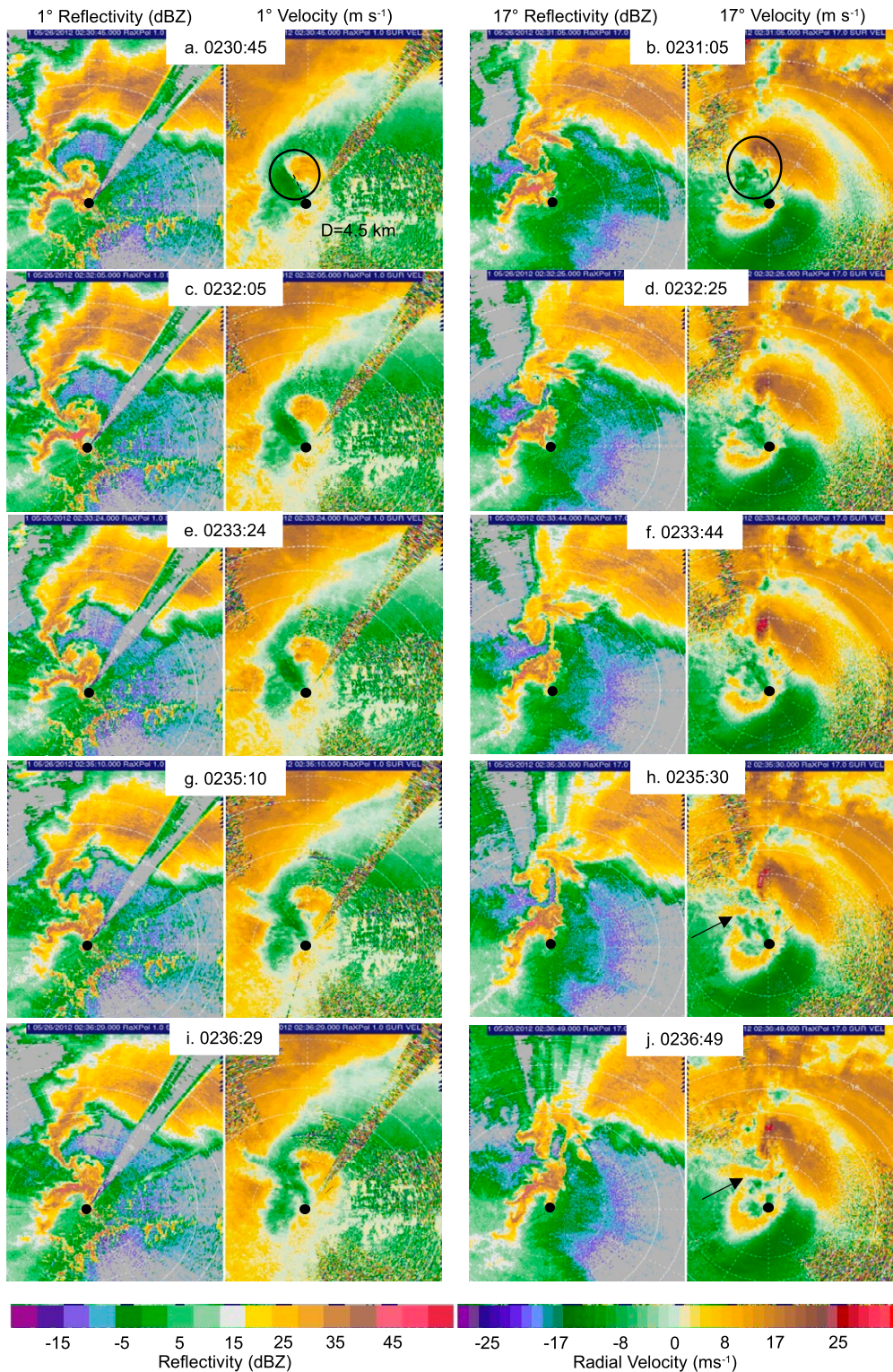


FIG. 9. (a)–(j) Evolution of the 25 May 2012 storm leading up to genesis of tornado 2 (which occurred between 0236 and 0237 UTC). Reflectivity (dBZ) at 1°, radial velocity (m s<sup>-1</sup>) at 1°, reflectivity (dBZ) at 17°, and radial velocity (m s<sup>-1</sup>) at 17°, shown in columns from left to right. Scan times are indicated next to the panel letter (UTC). TVS heights range from ~73 to 90 m (1.15–2 km) ARL for the 1° (15°) scans. Black circles in (a) and (b) draw attention to the mesocyclone, and arrows in (h) and (j) point to an area of divergence.

within the storm and new mesocyclone formation often occurred preferentially in one geographic location while the old ones moved away (see the online supplemental material animation). Because there were multiple tornadoes during this deployment, we refer to the tornadoes analyzed as TV1–5 in an effort to maintain organization and clarity.

A confirmed short-lived EF1 tornado (SPC ONETOR; SPC 2020) (TV1) was ongoing at the start of data collection (2305 UTC) (Figs. 3c and 11), but it quickly decayed. The TVS was vertically shallow, barely extending above 500 m, suggesting that this tornado might have been confined to the boundary layer (Figs. 6g–i and 11), although, it is again possible that tornado-strength rotation was present above the maximum observed height of ~1.2 km. TVs 2–5 formed following a classic cyclical pattern, with old vortices moving west or southwestward in a storm relative sense, while new mesocyclones formed to the east (Adlerman et al. 1999), producing subsequent tornadoes (see the online supplemental material). The timeframe of the tornadoes is given in Table 1. It is worth noting that TV3 formed in an area partially blocked by ground clutter from nearby hills, so the TVS was not well resolved and sometimes was entirely obscured in the lowest elevation angle data. The velocity estimates near the ground were likely biased low due to ground clutter at the lowest elevation angles. The final tornado (TV5) was documented visually by several of the authors and had an obvious condensation funnel in contact with the ground (Fig. 3d). However, there is no formal report for this tornado (or for TVs 2–4) in the SPC ONETOR database (SPC 2020), despite the visual documentation and the presence of a clear weak echo hole, tornado-strength TVS, and low correlation coefficient values associated with a TDS in the radar data (Fig. 12), likely owing to the remote, inaccessible location of the tornado and the relatively open country over which it occurred.

All tornadoes on this day had velocity signatures that were most discernable at low levels (e.g., Figs. 11 and 12). At higher elevation angles, there tended to be weak (non-tornado strength) vortices, but these vortices were distributed over a larger spatial scale than the tornado (4–5 km) and did not appear to evolve in an organized manner that would suggest they were associated with the tornado (e.g., Fig. 12e). There was no rotation around a central axis, nor was there consistent translation in any specific direction.

In three tornadogenesis cases observed by RaXPol this day (TV2, TV3, TV5), the evolution of the TVS regardless of the criterion employed, the  $\Delta V_{\max}$  and the  $\zeta_p$  all suggest a process of simultaneous (or nearly so) convergence over the lowest 1 km associated with genesis of the tornadoes (Figs. 6g–i, Figs. 7c and Figs. 8c). One case (TV4) suggests a rapid [ $O(<1)$  min] top-down process may have occurred. The observations of cyclic tornadogenesis by Dowell and Bluestein (2002) also suggested rapid evolution and development.

Although not the primary scope of this paper, all tornadoes on this day exhibited a top-down decay process (Figs. 6g,i), with decay occurring aloft first, similar to what was observed earlier this day by Griffitt et al. (2019) and in the 9 May 2016 Sulphur, Oklahoma, storm analyzed by McKeown et al. (2020). All five tornadoes appeared to be shallow with TVSS terminating at heights between ~500 m and 1 km. The final

vortex was the deepest and strongest, although it did not have a TVS in the top two elevation angles during its lifetime. Although the vertical domain terminated at ~2 km; there were no instances where a TVS was present in the highest elevation angle data except just prior to the genesis of TV4, and this TVS was only observed for one volume (Figs. 6g–i). Nor was there evidence to suggest downward descent from above the sampling domain. There may or may not have been tornadic rotation above this height, but there was definitely a dearth of strong rotation between ~1 and 2 km ARL, while there were visual observations of tornadoes associated with strong near ground rotation confined to heights < 1 km.

### c. 22 May 2016

On this day, RaXPol deployed at 2316 UTC, in the forward-flank precipitation area, resulting in attenuation and signal degradation of the hook echo, which was about 15 km away. Reflectivity features are poorly resolved as a result, but the radial velocities are still useful since they are not affected by signal attenuation unless the signal becomes extinct. The greater distance to the tornado allowed for observations to be collected through 5–6 km ARL, providing higher confidence in the sense of vertical evolution for this case than some of the earlier cases.

Several minutes prior to tornadogenesis, which occurred around 2351 UTC, a large hook echo was evident in the 2° elevation angle data (~600 m ARL), but cyclonic shear was broad and relatively weak, and the wind field was not well organized (Fig. 13). Higher, at 18° (~4.5 km ARL) the mesocyclone also was disorganized, although it was quite large, with nearly 10 km separating the maximum inbound and outbound velocities. Between the maxima, however, there were multiple areas with weak to moderate cyclonic shear. Some of these shear zones briefly spun up to tornado-strength, but they were transient.

Between 2348 and 2350 UTC, a surge of inbound velocities (the source of which was not investigated herein) appeared on the southern side of the hook echo at low levels (<2 km ARL) which significantly strengthened the low-level rotation (Fig. 13g). Over these two minutes, the low-level rotation intensified and converged, and tornadogenesis occurred shortly thereafter, between 2350 and 2351 UTC (Figs. 13g–i and 14). This tornado was formally reported and confirmed to be an EF2 (SPC ONETOR<sup>6</sup>; SPC 2020), although we could not visually discern it from our vantage point owing to intervening precipitation.

The time–height evolution of the TVSS identified using both criteria 1a/1b and 2 suggest nearly simultaneous contraction of the vortex over the lowest 1.5 km (Figs. 6j,k). Criterion 3 is not insightful, as the distances between the max inbound and outbound velocities were large, which reduced values of  $\zeta_p$  below the “tornadic” threshold for nearly the entire analysis period (Figs. 6l and 8d). The distance between velocity maxima distinctly increased with height (Fig. 14) and the flow field transitioned from having a well-organized single vortex

<sup>6</sup> The genesis time was reported as 2344 UTC, according to NWS damage survey (Storm Data). It is apparent from the radar observations that the actual genesis time was several minutes later.

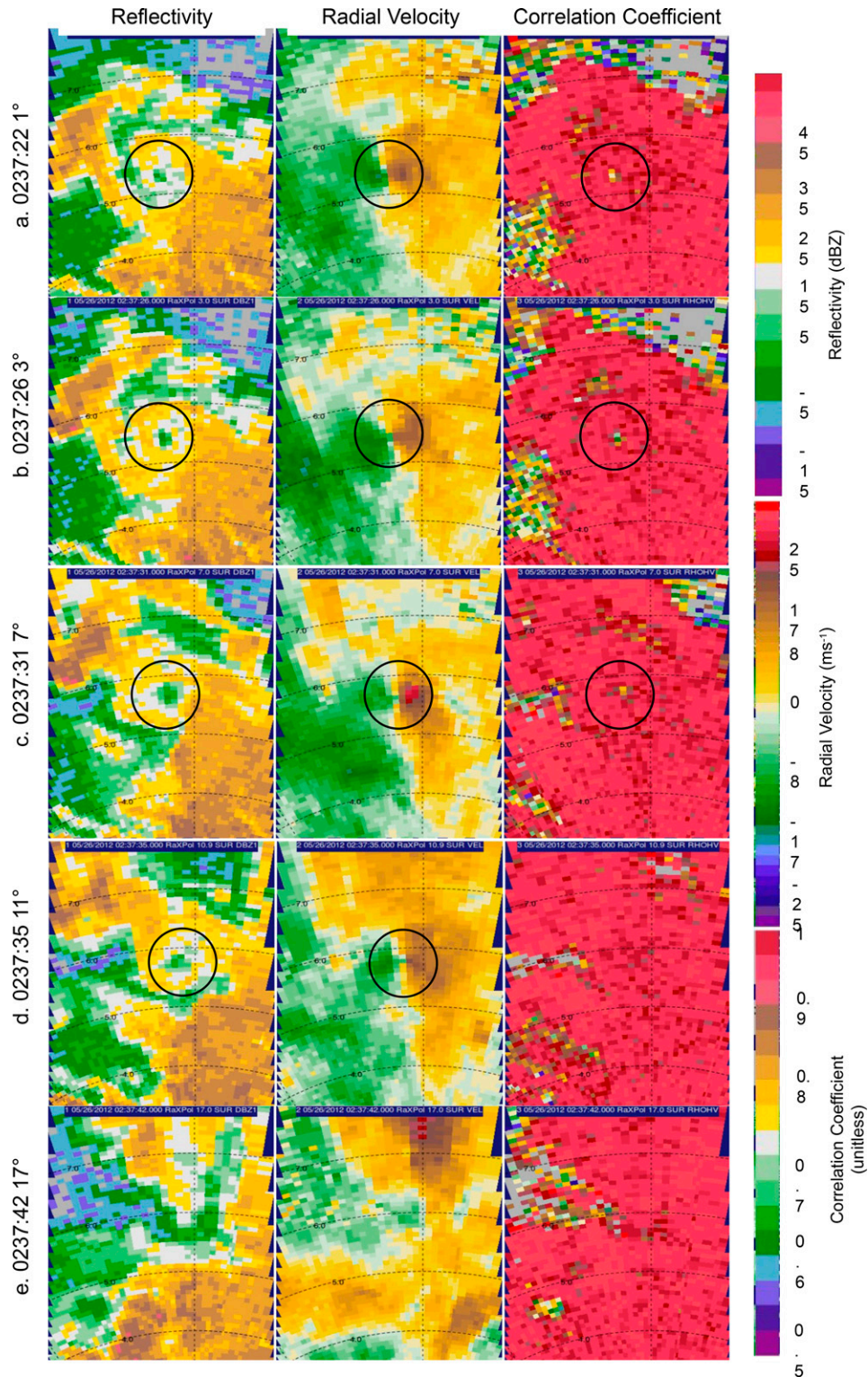


FIG. 10. (left) Reflectivity (dBZ), (center) radial velocity ( $\text{m s}^{-1}$ ), and (right) correlation coefficient (unitless) images from select elevations for the volume scan at the time of tornadogenesis in the second tornado of 25 May 2012. (a)  $1^\circ$  (90 m), (b)  $3^\circ$  (280 m), (c)  $7^\circ$  (700 m), (d)  $11^\circ$  (1.1 km), and (e)  $17^\circ$  (2 km). Range rings are provided every 1 km. Open black circles denote the locations of the weak echo hole in the left column, the TVS in the center column, and the TDS in the right column.

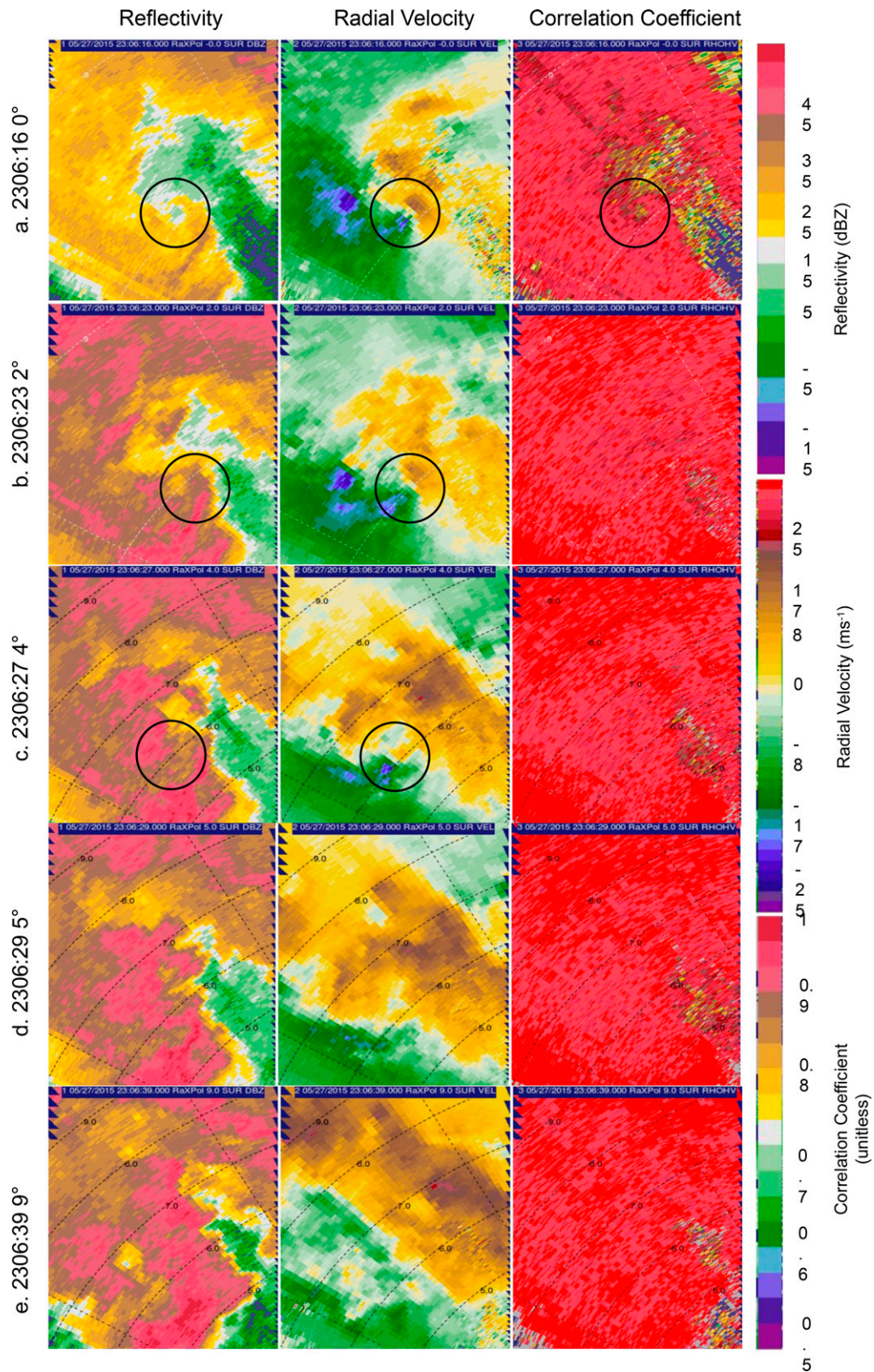


FIG. 11. As in Fig. 10, but for the tornado TV1 at 2306 UTC 27 May 2015, and for (a) 0° (~10 m), (b) 2° (~220 m), (c) 4° (~440 m), (d) 5° (~540 m), and (e) 9° (~1 km) elevation angles. The parenthetical heights are ARL given for the approximate center of the TVS.

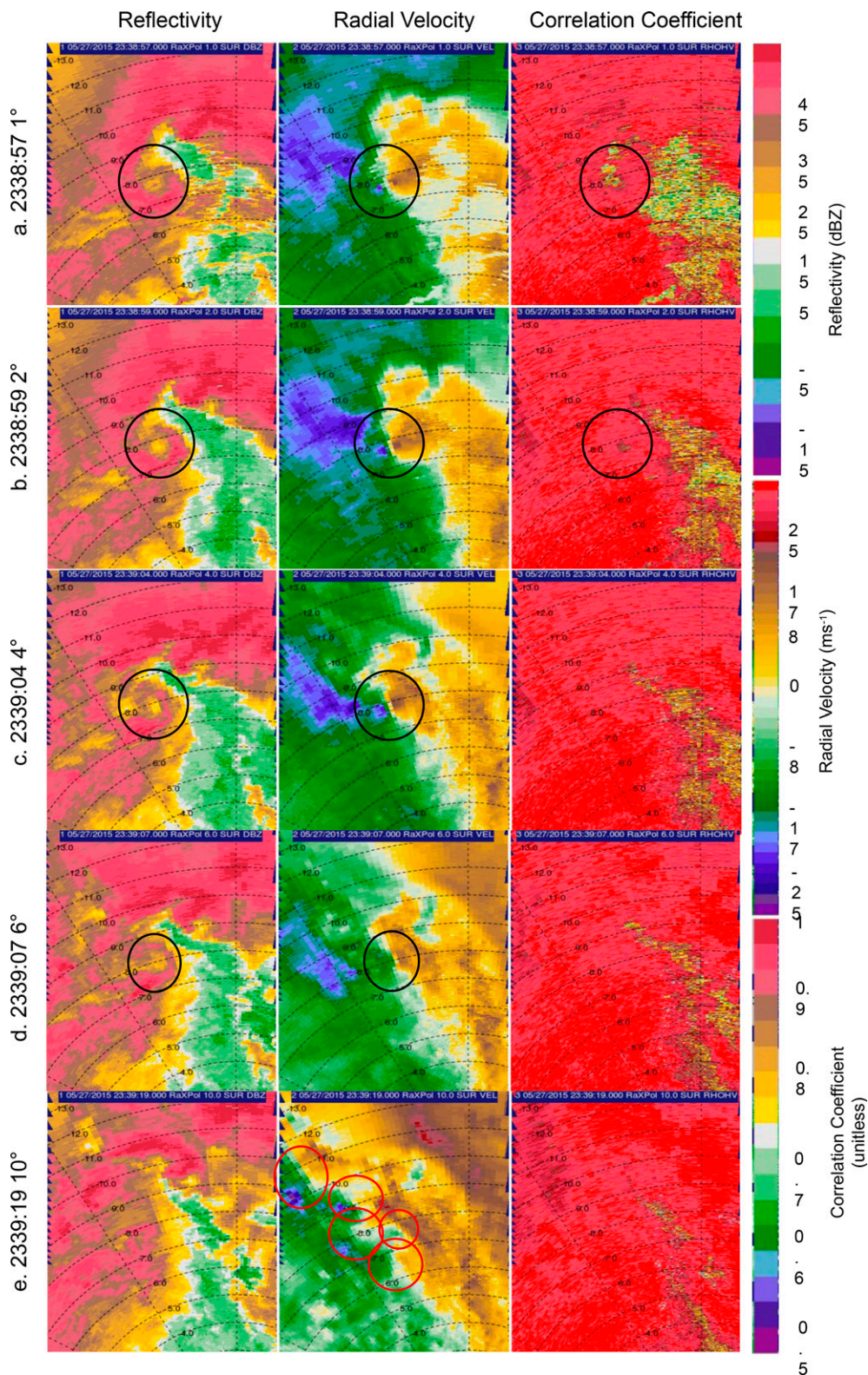


FIG. 12. As in Fig. 10, but for the tornado TV5 at 2339 UTC 27 May 2015, and for (a) 1° (~175 m), (b) 2° (~270 m), (c) 4° (~580 m), (d) 6° (~800 m), and (e) 10° (~1.4 km) elevation angles (heights ARL). Black circles indicate the location of the tornado while red circles denote smaller-scale regions of rotation associated with a multiple-vortex-like mesocyclone structure.

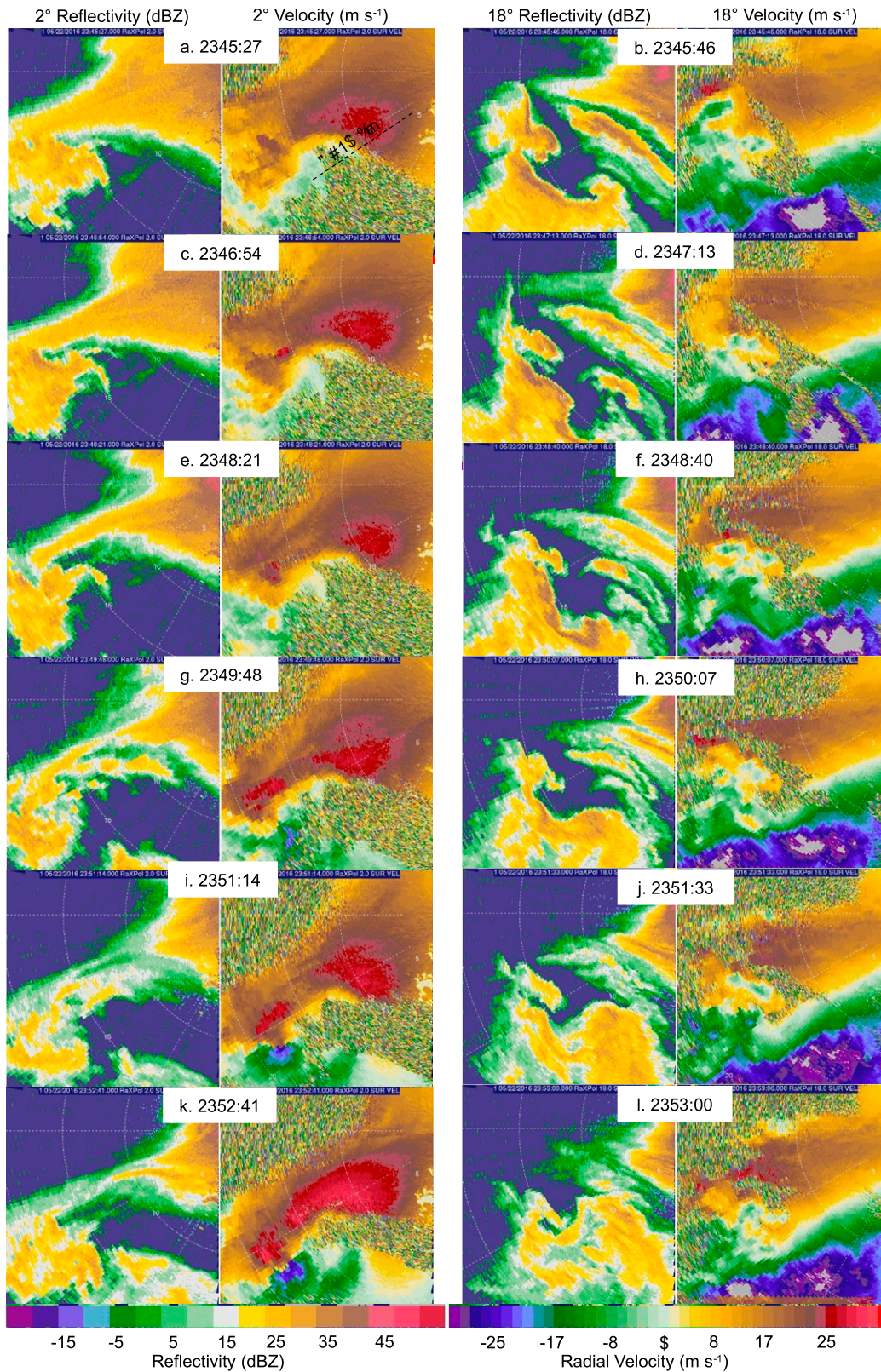


FIG. 13. As in Fig. 9, but for the tornado on 22 May 2016. (left) From 2° and (right) from 18°. Heights near the center of the TVSS ranged from ~580 to 620 m (5–5.5 km) ARL for the 2° (18°) scans. Gray pixels exceed the color bar. RaXPoI is deployed to the top right of the image, out of the range of the figure.

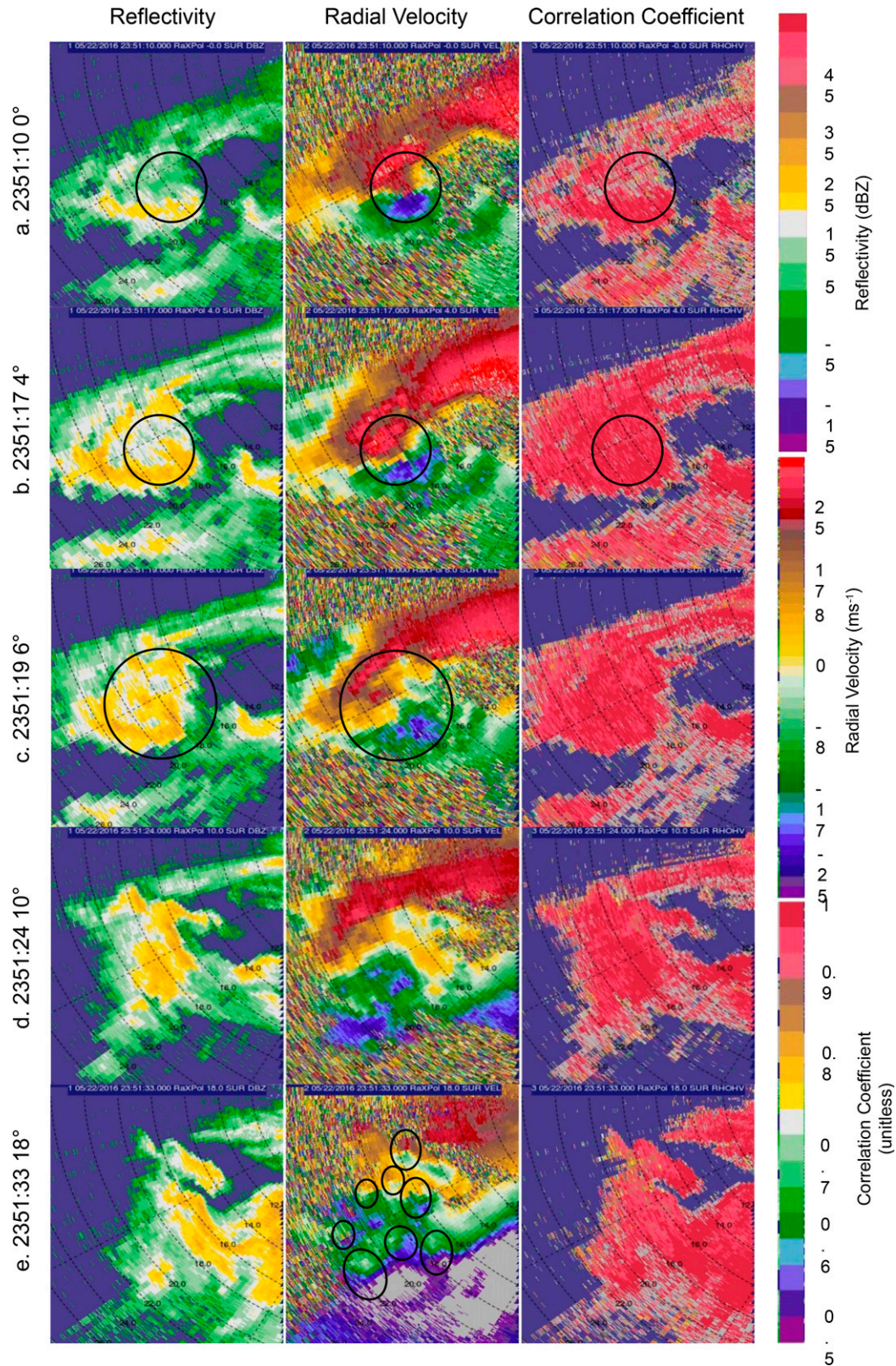


FIG. 14. As in Fig. 10, but for the tornado at 2351 UTC 22 May 2016, and for (a) 0° (~10 m), (b) 4° (~1.3 km), (c) 6° (~2 km), (d) 10° (~3.2 km), and (e) 18° (~5.1 km) elevation angles. Heights are for approximate TVS center locations and are given in ARL.

to becoming much more turbulent, with no evidence of the ongoing tornado (Figs. 13j,l), similar to what was seen on 27 May 2015. In fact, the wind field at 18° had many weak cyclonic vortices (Fig. 14e), resembling a multiple-vortex mesocyclone (Wurman and Kosiba 2013).

The TVSs remained confined to heights below 2 km (observations were collected through ~5 km ARL at this time) for more than 3 min before the development of a deep, vertically coherent vortex, similar to what was observed in the 31 May 2013 El Reno, Oklahoma, tornado (Bluestein et al. 2019) although in that case, the vortex was even shallower. Following this, the spatiotemporal evolution of the TVSs and  $\Delta V_{\max}$ s suggests a bottom-up process of intensification as the deeper vortex developed (Figs. 6j,k and 7d). When looking at the values of  $\Delta V_{\max}$ , it is evident that this case had stronger rotation than any of the other cases (Fig. 7d). Observations at higher altitudes had  $\Delta V_{\max}$  values that exceeded the 40 m s<sup>-1</sup> criterion, but the velocity maxima were more than 2 km apart, thereby disqualifying the couplet from being considered a TVS. The  $\zeta_p$  was generally greatest at heights < 2 km except for when there were small-scale transient vortices aloft (Fig. 8d).

There was photographic evidence acquired from storm chasers of a condensation funnel in contact with the ground at 2352 UTC, prior to the development of the vertically deep vortex (Fig. 3e), but during the timeframe over which shallow, (i.e.,  $z < 2$  km) low-level tornadic rotation was identified herein. The tornado persisted for at least 15 more minutes, and was still ongoing when the radar deployment ended at 0005 UTC 23 May.

In summary, this tornado was the strongest, widest, and longest-lived out of the seven studied herein, and it had the most vertically complete observational domain (i.e., from a few tens of meters through ~6 km ARL) of all the cases. It formed in a non-descending manner (at least as ascertained by the 30-s time interval over which new volume updates were obtained), nearly simultaneously, over the lowest 1.5 km ARL. However, we cannot rule out some sort of very fast, although vertically shallow, top-down process that is indiscernible from our ~30-s volume updates. The vortex was initially confined to this depth for nearly 5 min until it rapidly intensified from 1.5 km upward through the top of the vertical domain (~5 km ARL).

## 5. Discussion

Five of the seven tornadogenesis cases studied herein suggest a non-descending and rapidly intensifying pattern of evolution in the velocity field while one case appears to indicate a rapid top-down process and the interpretation of another is dependent upon the criterion used to define a TVS, or the parameter used (e.g., TVS vs  $\Delta V_{\max}$  vs  $\zeta_p$ ). Six out of the seven cases had modest to strong near-ground rotation on the order of 1–3 min prior to tornadogenesis. These results agree well with other recent numerical and observational studies of tornadogenesis (e.g., French et al. 2013; Kosiba et al. 2013; Schenkman et al. 2014; Houser et al. 2015; Mashiko 2016; Markowski 2016; Markowski et al. 2018; Yokota et al. 2018;

Bluestein et al. 2019; Wienhoff et al. 2020) and support the hypothesis that strong, a priori near-ground vorticity is important to tornado formation. In the context of the broader tornadogenesis process, prior to the development of strong, near-ground rotation, a strengthening low-level mesocyclone which induces an upward-directed perturbation pressure gradient force could be responsible for converging high angular momentum air underneath the low-level mesocyclone at near-ground heights. However, a strong low-level mesocyclone would be required to overcome the downward-directed perturbation pressure gradient force associated with the near-ground rotation in order to stretch and amplify the near-ground vorticity into a tornado. If near-ground air has low angular momentum initially, a large low-level mesocyclone induced pressure deficit also would be required to drive the updraft necessary to converge ambient vorticity to tornadic intensity.

For tornado 1 on 25 May 2012 in which non-descending evolution was questionable, it is possible that this was an artifact caused by low-biased radial velocities due to the small diameter of the tornado at near-ground levels and the relatively far range from the radar. Near ground sub-tornadic strength rotation was present and was juxtaposed with the location of the tornadic-strength rotation above. Had this rotation met the  $\Delta V_{\max}$  criteria imposed herein, this vortex would have been classified as non-descending. However, it is also possible that a rapid [ $O(1-2)$  min] top-down process did actually occur, as was also suggested during the genesis of TV4 on 27 May 2015.

Another unintended result found from this study was the limited vertical extent of many of the tornadoes. Only two of the eight tornadoes examined (tornado 1 from 25 May 2012 and the 22 May 2016 tornado) appeared to be deep and vertically coherent over the analysis timeframe. The early stages of tornado 2 on 25 May 2012 had a TVS that terminated around 1.5 km AGL, and all of the weak tornadoes occurring on 27 May 2015 weakened at heights < 1.25 km ARL and TVSs were absent in nearly all observations from the upper two elevation angles. Furthermore, TV1 and TV2 on 27 May 2015 were entirely limited to heights < 700 m, although the deployment began a minute or two after genesis of TV1 occurred. However, the vertical extent of our domain was not sufficiently deep for these six tornadoes to conclude that tornado-strength rotation was not present above the height at which these vortices appear to terminate in the RaXPol data. Therefore, we cannot determine whether the upper limits of the TVSs observed herein represent a true terminus of the vortex. It is possible that the lack of TVSs may instead correspond with a strongly tilted vortex (i.e., nearly parallel to the ground) or an inversion layer, or “cap,” that has been found in other instances to be a location of weak or non-existent rotation near this height (e.g., French et al. 2013; Houser et al. 2015; Bluestein et al. 2019; Wienhoff et al. 2020). However, on 22 May 2016, when vertical sampling exceeded 5 km ARL, a tornado associated with a shallow TVS was photographed at 2352 UTC (Fig. 3e), 3 min prior to the development of the deep tornado vortex. The radar-observed low-level TVS at this time terminated at a height < 1.5 km ARL and the

TABLE 2. Summary of tornadogenesis evolution [non-descending (ND) or descending (D)] based upon the various different techniques employed. Criterion 1 (Crit 1):  $\Delta V_{\max} > 40 \text{ m s}^{-1}$  with  $<2 \text{ km}$ , as long as there are no more than 3 radials separating  $\Delta V_{\max} > 40 \text{ m s}^{-1}$  OR  $\zeta_p$  that was  $>0.1 \text{ s}^{-1}$ , as long as  $\Delta V > 30 \text{ m s}^{-1}$ . Criterion 2 (Crit 2): Any  $\Delta V_{\max} > 30 \text{ m s}^{-1}$ . Criterion 3 (Crit 3): Any  $\zeta_p$  that was  $>0.1 \text{ s}^{-1}$  as long as  $\Delta V_{\max} > 20 \text{ m s}^{-1}$ . Here,  $\Delta V_{\max}$ : Evaluation based upon all heights and all values of  $\Delta V_{\max}$ ;  $\zeta_p$ : Evaluation based upon all heights and all values of  $\zeta_p$ . ND\* indicates predominately non-descending evolution, with some indication of descent in the lowest 500 m. For Tor 1 25 May 2012  $\zeta_p$ , above 500 m evolution is non-descending, however, below 500 m, evidence of descending. For Tor 2 25 May 2012 Crit 1, general non-descending trend over lowest 1.5 km, but below 500 m, possible descending trend. For TV2, missing data near the ground precludes an analysis below 250 m, but the general trend appears non-descending. The N/A for Crit 3 on 22 May 2016 is because the  $\zeta_p$  never reached the “tornadic” threshold.

Date	Crit 1	Crit 2	Crit 3	$\Delta V_{\max}$	$\zeta_p$
25 May 2012 Tor 1	D	D	ND	ND	ND*
25 May 2012 Tor 2	ND*	ND	ND	ND	ND
27 May 2015 TV2	ND*	ND*	ND	ND	ND
27 May 2015 TV3	ND	ND	ND	ND	ND
27 May 2015 TV4	D	D	ND	ND	ND
27 May 2015 TV5	ND	ND	ND	ND	ND
22 May 2016	ND	ND	N/A	ND	N/A

shallow vortex was present for nearly 5 min prior to the development of the deep vortex. Since data were collected through a height of 5 km for this case, it is assumed that 1.5 km is the actual terminus height of the tornado photographed in Fig. 3e, which was taken at a time when the radar observed the shallow vortex. A shallow vortex having a visible condensation funnel in contact with the ground was also observed in the 31 May 2013 El Reno tornado (Bluestein et al. 2019). We therefore believe that it is possible these tornadoes truly were as shallow as we are reporting.

## 6. Conclusions

This study investigated the spatiotemporal evolution of rotation associated with tornadogenesis in seven tornadoes that formed within supercells, using observations from a rapid-scan, mobile, radar (RaXPoI). All of these tornadoes were observed at heights below 200 m, and six had observations from the 0° elevation angle, representing a bore-site beam elevation a few tens of meters above the radar level. The relatively dense near-ground observations acquired in these cases made it possible to investigate the time–height evolution of near-ground tornadic rotation during genesis. A summary of the results is given in Table 2. From analysis of these cases, three conclusions are drawn:

- 1) Five out of the seven tornadoes for which genesis was captured had TVS,  $\Delta V_{\max}$ , and  $\zeta_p$  trends that distinctly followed a non-descending pattern of evolution during genesis over the lowest 2 km ARL (the vertical domain for which radar data were consistently available) (Table 2).

One tornado appeared to form via a rapid [i.e.,  $O(<60) \text{ s}$ ] descending process, while the interpretation of another tornado’s vertical evolution was dependent upon the criterion and parameter used to define tornadogenesis. Four of these seven tornadoes (three of which were determined to be non-descending, one of which was descending) occurred from the same cyclic parent supercell. Thus, our sample is biased towards the overarching conditions associated with this one storm.

- 2) Interpretation of the spatiotemporal evolution of the TVS can vary depending upon the criterion employed to define a velocity couplet as being “tornadic” (Table 2). The first 25 May 2012 tornado was analyzed as having top-down evolution according to criteria 1a/1b and 2, while it was non-descending according to criterion 3. The evolution of the second 25 May 2012 tornado TVS at heights  $< 500 \text{ m}$  was also dependent upon which criterion was employed, although that vortex suggested a non-descending pattern over the depth of observations. This conclusion has substantially serious implications for current and future work trying to best determine when a velocity couplet is a “TVS,” as it proves that the interpretation of results may be a function of the methodology, and it raises the question of when rotation should be considered “tornadic.”
- 3) Six out of the seven tornadoes analyzed plus the additional tornado for which genesis was not captured (on 27 May 2015) had TVSs that terminated at heights  $< 2 \text{ km}$  ARL for at least several minutes after genesis. However, this conclusion should be viewed with some caution, as limitations in the vertical extent of observations in six of the eight cases precluded the identification of TVSs above 2–2.5 km. Thus, while there is a dearth of TVSs between 1.5 and 2 km ARL, this does not necessarily imply TVSs are non-existent above this height. However, it can be stated with certainty that the 22 May 2016 tornado was confined to heights  $< 2 \text{ km}$  ARL for at least 3 minutes.

In all of the tornadogenesis cases, except for the 25 May 2016 tornado, strong (tornadic or sub-tornadic) rotation was present at (or very near) the ground prior to the development of a deeper vortex. For all cases, tornadogenesis occurred over time scales on the order of  $\sim 1 \text{ min}$  or less. These analyses provide additional observational evidence that tornadogenesis is a very rapid process, and, at least in some cases, TVSs likely do not descend with time as a tornado forms. It is important to note, however, our sample size is still quite small and does not represent a thorough distribution of the observed range of tornado intensities, structures, or environments. Of particular consequence is the fact that 4 of the observed tornadogenesis cases came from the same cyclic parent supercell. It has been noted in prior studies that tornadogenesis occurring subsequently to the initial tornado formed by a cyclic supercell often is more rapid than genesis associated with the first tornado, and the near ground environment may already be “primed” to for tornado formation (e.g., Burgess et al. 1982). Thus, our results should be interpreted

as being case specific rather than generalizable to all tornadoes. We should also note that we are basing our conclusions on the evolution of the TVS and its associated maximum differential velocity and  $\zeta_p$ . This does not necessarily represent the pattern of other tornado features. For example, funnel clouds, which are a function of not only the wind field, but also the thermodynamic characteristics, do not conform to this evolution. Similarly, the pressure deficit associated with the tornadic rotation may not evolve in this manner either (e.g., Orf et al. 2017).

In conclusion, this study investigated tornadogenesis in seven tornadoes using a variety of different criteria which generally supported non-descending evolution in mesocyclonic tornadogenesis, adding valuable additional case studies to the scientific literature on this topic. Still, more work needs to be done, particularly to include a greater diversity of tornadoes and environments, and with deeper sample volumes through at least 5 km ARL.

**Acknowledgments.** We acknowledge the support of NSF Grants AGS-0934307, AGS-0821231, AGS-1262048, AGS-1560945, AGS-1749504, and AGS-1947146; and we also acknowledge the contributions made to this work by storm chasers and photographers Alec Scholten and Ashton Robinson Cook, as well as ARRC personnel John Meier, Boon-Leng Cheong, Danny Feland, Tian Yu, and Bob Palmer. We further acknowledge the contributions of Drs. Mike French, Leigh Orf, Anton Seimon, and John Allen who engaged in valuable discussions with the first author about non-descending tornadogenesis that aided in the analysis and interpretation of this work. Furthermore, we acknowledge the contributions of the anonymous reviewers who provided constructive feedback and recommendations on how to improve this manuscript and the study.

## REFERENCES

- Adlerman, E. J., K. K. Droegemeier, and R. Davies-Jones, 1999: A numerical simulation of cyclic mesocyclogenesis. *J. Atmos. Sci.*, **56**, 2045–2069, [https://doi.org/10.1175/1520-0469\(1999\)056<2045:ANSOCM>2.0.CO;2](https://doi.org/10.1175/1520-0469(1999)056<2045:ANSOCM>2.0.CO;2).
- Alexander, C., and J. Wurman, 2008: Updated mobile radar climatology of supercell tornado structures and dynamics. *24th Conf. on Severe Local Storms*, Savannah, GA, Amer. Meteor. Soc., 19.4, [https://ams.confex.com/ams/24SLS/techprogram/paper\\_141821.htm](https://ams.confex.com/ams/24SLS/techprogram/paper_141821.htm).
- Bluestein, H. B., 1985: The formation of a “landspout” in a “broken-line” squall line in Oklahoma. Preprints, *14th Conf. on Severe Local Storms*, Indianapolis, IN, Amer. Meteor. Soc., 267–270.
- , 2022: Observations of tornadoes and their parent supercells using ground-based, mobile Doppler radars. *Remote Sensing and Natural Hazards*, K. Zhang, Y. Hong, and A. AghaKouchak, Eds., John Wiley and Sons, 31–67.
- , C. Weiss, and A. L. Pazmany, 2003: Mobile Doppler radar observations of a tornado in a supercell near Bassett, Nebraska, on 5 June 1999. Part I: Tornadogenesis. *Mon. Wea. Rev.*, **131**, 2954–2967, [https://doi.org/10.1175/1520-0493\(2003\)131<2954:MDROOA>2.0.CO;2](https://doi.org/10.1175/1520-0493(2003)131<2954:MDROOA>2.0.CO;2).
- , M. M. French, R. L. Tanamachi, S. Frasier, K. Hardwick, F. Junyent, and A. L. Pazmany, 2007: Close-range observations of tornadoes in supercells made with a dual-polarization, X-band, mobile Doppler radar. *Mon. Wea. Rev.*, **135**, 1522–1543, <https://doi.org/10.1175/MWR3349.1>.
- , —, I. Popstefanija, R. T. Bluth, and J. B. Knorr, 2010: A mobile, phased-array Doppler radar for the study of severe convective storms. *Bull. Amer. Meteor. Soc.*, **91**, 579–600, <https://doi.org/10.1175/2009BAMS2914.1>.
- , K. J. Thiem, J. C. Snyder, and J. B. Houser, 2019: Tornado genesis and early tornado evolution in the El Reno, Oklahoma, supercell on 31 May 2013. *Mon. Wea. Rev.*, **147**, 2045–2066, <https://doi.org/10.1175/MWR-D-18-0338.1>.
- Brady, R. H., and E. J. Szoke, 1989: A case study of non-mesocyclone tornado development in Northeast Colorado: Similarities to waterspout formation. *Mon. Wea. Rev.*, **117**, 843–856, [https://doi.org/10.1175/1520-0493\(1989\)117<0843:ACSONT>2.0.CO;2](https://doi.org/10.1175/1520-0493(1989)117<0843:ACSONT>2.0.CO;2).
- Brown, R. A., and V. T. Wood, 2012: The tornadic vortex signature: An update. *Wea. Forecasting*, **27**, 525–530, <https://doi.org/10.1175/WAF-D-11-00111.1>.
- , L. R. Lemon, and D. W. Burgess, 1978: Tornado detection by pulsed Doppler radar. *Mon. Wea. Rev.*, **106**, 29–38, [https://doi.org/10.1175/1520-0493\(1978\)106<0029:TDBPDR>2.0.CO;2](https://doi.org/10.1175/1520-0493(1978)106<0029:TDBPDR>2.0.CO;2).
- Bryan, G., and J. M. Fritsch, 2002: A benchmark simulation for moist nonhydrostatic numerical models. *Mon. Wea. Rev.*, **130**, 2917–2928, [https://doi.org/10.1175/1520-0493\(2002\)130<2917:ABSFMN>2.0.CO;2](https://doi.org/10.1175/1520-0493(2002)130<2917:ABSFMN>2.0.CO;2).
- Burgess, D. W., and R. J. Donaldson, 1979: Contrasting tornadic storm types. Preprints, *11th Conf. on Severe Local Storms*, Kansas City, KS, Amer. Meteor. Soc., 189–192.
- , L. R. Lemon, and R. A. Brown, 1975: Tornado characteristics revealed by Doppler radar. *Geophys. Res. Lett.*, **2**, 183–184, <https://doi.org/10.1029/GL002i005p00183>.
- , V. T. Wood, and R. A. Brown, 1982: Mesocyclone evolution statistics. Preprints, *12th Conf. on Severe Local Storms*, San Antonio, TX, Amer. Meteor. Soc., 422–424.
- Cai, H., 2005: Comparison between tornadic and nontornadic mesocyclones using the vorticity (pseudovorticity) line technique. *Mon. Wea. Rev.*, **133**, 2535–2551, <https://doi.org/10.1175/MWR2990.1>.
- Dahl, J. M. L., 2015: Near-ground rotation in simulated supercells: On the robustness of the baroclinic mechanism. *Mon. Wea. Rev.*, **143**, 4929–4942, <https://doi.org/10.1175/MWR-D-15-0115.1>.
- , M. D. Parker, and L. J. Wicker, 2014: Imported and storm-generated near-ground vertical vorticity in a simulated supercell. *J. Atmos. Sci.*, **71**, 3027–3051, <https://doi.org/10.1175/JAS-D-13-0123.1>.
- Donaldson, R. J., 1978: Observations of the Union City tornadic storm by plan shear indicator. *Mon. Wea. Rev.*, **106**, 39–47, [https://doi.org/10.1175/1520-0493\(1978\)106<0039:OOTUCT>2.0.CO;2](https://doi.org/10.1175/1520-0493(1978)106<0039:OOTUCT>2.0.CO;2).
- Doviak, R. J., and D. S. Zrnić, 1993: *Doppler Radar and Weather Observations*. 2nd ed. Academic Press, 562 pp.
- Dowell, D., and H. B. Bluestein, 2002: The 8 June 1995 McLean, Texas, storm. Part II: Cyclic tornado formation, maintenance, and dissipation. *Mon. Wea. Rev.*, **130**, 2649–2670, [https://doi.org/10.1175/1520-0493\(2002\)130<2649:TJMTSP>2.0.CO;2](https://doi.org/10.1175/1520-0493(2002)130<2649:TJMTSP>2.0.CO;2).
- French, M. M., H. B. Bluestein, I. Popstefanija, C. A. Baldi, and R. T. Bluth, 2013: Reexamining the vertical development of

- tornadic vortex signatures in supercells. *Mon. Wea. Rev.*, **141**, 4576–4601, <https://doi.org/10.1175/MWR-D-12-00315.1>.
- , —, —, —, and —, 2014: Mobile, phased-array, Doppler radar observations of tornadoes at X band. *Mon. Wea. Rev.*, **142**, 1010–1036, <https://doi.org/10.1175/MWR-D-13-00101.1>.
- Grasso, L. D., and W. R. Cotton, 1995: Numerical simulation of a tornado vortex. *J. Atmos. Sci.*, **52**, 1192–1203, [https://doi.org/10.1175/1520-0469\(1995\)052<1192:NSOATV>2.0.CO;2](https://doi.org/10.1175/1520-0469(1995)052<1192:NSOATV>2.0.CO;2).
- Griffin, C., D. J. Bodine, J. M. Kurdzo, A. Mahre, and R. D. Palmer, 2019: High-temporal resolution observations of the 27 May 2015 Canadian, Texas, tornado using the atmospheric imaging radar. *Mon. Wea. Rev.*, **147**, 873–891, <https://doi.org/10.1175/MWR-D-18-0297.1>.
- Houser, J. B., H. B. Bluestein, and J. C. Snyder, 2015: Rapid-scan, polarimetric, Doppler radar observations of tornadogenesis and tornado dissipation in a tornadic supercell: The “El Reno, Oklahoma” storm of 24 May 2011. *Mon. Wea. Rev.*, **143**, 2685–2710, <https://doi.org/10.1175/MWR-D-14-00253.1>.
- Inman, J., 1835: *Navigation and Nautical Astronomy: For the Use of British Seamen*. W. Woodward and C. & J. Rivington, 280 pp.
- Isom, B., and Coauthors, 2013: The atmospheric imaging radar: Simultaneous volumetric observations using a phased array weather radar. *J. Atmos. Oceanic Technol.*, **30**, 655–675, <https://doi.org/10.1175/JTECH-D-12-00063.1>.
- Johnson, K. W., P. S. Ray, B. S. Johnson, and R. P. Davies-Jones, 1987: Observations related to the rotational dynamics of the 20 May 1977 tornadic storms. *Mon. Wea. Rev.*, **115**, 2463–2478, [https://doi.org/10.1175/1520-0493\(1987\)115<2463:ORTTRD>2.0.CO;2](https://doi.org/10.1175/1520-0493(1987)115<2463:ORTTRD>2.0.CO;2).
- Klemp, J. B., and R. Rotunno, 1983: A study of the tornadic region within a supercell thunderstorm. *J. Atmos. Sci.*, **40**, 359–377, [https://doi.org/10.1175/1520-0469\(1983\)040<0359:ASOTTR>2.0.CO;2](https://doi.org/10.1175/1520-0469(1983)040<0359:ASOTTR>2.0.CO;2).
- Kosiba, K. A., and J. Wurman, 2013: The three-dimensional structure and evolution of a tornado boundary layer. *Wea. Forecasting*, **28**, 1181–1552, <https://doi.org/10.1175/WAF-D-13-00070.1>.
- , —, Y. P. Richardson, P. Markowski, and P. Robinson, 2013: Genesis of the Goshen County, Wyoming, tornado on 5 June 2009 during VORTEX2. *Mon. Wea. Rev.*, **141**, 1157–1181, <https://doi.org/10.1175/MWR-D-12-00056.1>.
- Kumjian, M. R., and A. V. Ryzhkov, 2008: Polarimetric signatures in supercell thunderstorms. *J. Appl. Meteor. Climatol.*, **47**, 1940–1961, <https://doi.org/10.1175/2007JAMC1874.1>.
- Kurdzo, J. M., D. J. Bodine, B. L. Cheong, and R. D. Palmer, 2015: High-temporal resolution polarimetric X-band Doppler radar observations of the 20 May 2013 Moore, Oklahoma, tornado. *Mon. Wea. Rev.*, **143**, 2711–2735, <https://doi.org/10.1175/MWR-D-14-00357.1>.
- , and Coauthors, 2017: Observations of severe local storms and tornadoes with the atmospheric imaging radar. *Bull. Amer. Meteor. Soc.*, **98**, 915–935, <https://doi.org/10.1175/BAMS-D-15-00266.1>.
- Lee, B. D., and R. B. Wilhelmson, 1997: The numerical simulation of nonsupercell tornadogenesis. Part II: Evolution of a family of tornadoes along a weak outflow boundary. *J. Atmos. Sci.*, **54**, 2387–2415, [https://doi.org/10.1175/1520-0469\(1997\)054<2387:TNSONT>2.0.CO;2](https://doi.org/10.1175/1520-0469(1997)054<2387:TNSONT>2.0.CO;2).
- , K. A. Finley, and C. D. Karstens, 2012: The Bowdle, South Dakota, cyclic tornadic supercell of 22 May 2010: Surface analysis of rear-flank downdraft evolution and multiple internal surges. *Mon. Wea. Rev.*, **140**, 3419–3441, <https://doi.org/10.1175/MWR-D-11-00351.1>.
- Leslie, L. M., 1971: The development of concentrated vortices: A numerical study. *J. Fluid Mech.*, **48**, 1–21, <https://doi.org/10.1017/S0022112071001435>.
- Markowski, P. M., 2016: An idealized numerical simulation investigation of the effects of surface drag on the development of near-surface vertical vorticity in supercell thunderstorms. *J. Atmos. Sci.*, **73**, 4349–4385, <https://doi.org/10.1175/JAS-D-16-0150.1>.
- , and Y. P. Richardson, 2014: The influence of environmental low-level shear and cold pools on tornadogenesis: Insights from idealized simulations. *J. Atmos. Sci.*, **71**, 243–275, <https://doi.org/10.1175/JAS-D-13-0159.1>.
- , T. P. Hatlee, and Y. P. Richardson, 2018: Tornadogenesis in the 12 May 2010 supercell thunderstorm intercepted by VORTEX2 near Clinton, Oklahoma. *Mon. Wea. Rev.*, **146**, 3623–3650, <https://doi.org/10.1175/MWR-D-18-0196.1>.
- Marquis, J., Y. Richardson, J. Wurman, and P. Markowski, 2008: Single- and dual-Doppler analysis of a tornadic vortex and surrounding storm-scale flow in the Crowell, Texas, supercell of 30 April 2000. *Mon. Wea. Rev.*, **136**, 5017–5043, <https://doi.org/10.1175/2008MWR2442.1>.
- , —, P. Markowski, D. Dowell, and J. Wurman, 2012: Tornado maintenance investigated with high-resolution dual-Doppler and EnKF analysis. *Mon. Wea. Rev.*, **140**, 3–27, <https://doi.org/10.1175/MWR-D-11-00025.1>.
- Mashiko, W., 2016: A numerical study of the 6 May 2012 Tsukuba City supercell tornado. Part II: Mechanisms of tornadogenesis. *Mon. Wea. Rev.*, **144**, 3077–3098, <https://doi.org/10.1175/MWR-D-15-0122.1>.
- , H. Niino, and T. Kato, 2009: Numerical simulation of tornadogenesis in an outer-rainband minisupercell of Typhoon Shanshan on 17 September 2006. *Mon. Wea. Rev.*, **137**, 4238–4260, <https://doi.org/10.1175/2009MWR2959.1>.
- McKeown, K. E., M. M. French, K. S. Tuftedal, D. M. Kingfield, H. B. Bluestein, D. W. Reif, and Z. B. Wienhoff, 2020: Rapid-scan and polarimetric radar observations of the dissipation of a violent tornado on 9 May 2016 near Sulphur, Oklahoma. *Mon. Wea. Rev.*, **148**, 3951–3971, <https://doi.org/10.1175/MWR-D-20-0033.1>.
- Mitchell, E. D., S. V. Vasiloff, G. J. Stumpf, A. Witt, M. D. Eilts, J. T. Johnson, and K. W. Thomas, 1998: The National Severe Storms Laboratory tornado detection algorithm. *Wea. Forecasting*, **13**, 352–366, [https://doi.org/10.1175/1520-0434\(1998\)013<0352:TNSSLT>2.0.CO;2](https://doi.org/10.1175/1520-0434(1998)013<0352:TNSSLT>2.0.CO;2).
- Murdzek, S. S., P. M. Markowski, and Y. P. Richardson, 2020: Processes preventing the development of a significant tornado in a Colorado supercell on 26 May 2010. *Mon. Wea. Rev.*, **148**, 1753–1778, <https://doi.org/10.1175/MWR-D-19-0288.1>.
- Naylor, J., and M. Gilmore, 2014: Vorticity evolution leading to tornadogenesis and tornadogenesis failure in simulated supercells. *J. Atmos. Sci.*, **71**, 1201–1217, <https://doi.org/10.1175/JAS-D-13-0219.1>.
- Noda, A., and H. Niino, 2010: A numerical investigation of a supercell tornado: Genesis and vorticity budget. *J. Meteor. Soc. Japan*, **88**, 135–159, <https://doi.org/10.2151/jmsj.2010-203>.
- Orf, L., R. Wilhelmson, B. Lee, C. Finley, and A. Houston, 2017: Evolution of a long-track violent tornado within a simulated supercell. *Bull. Amer. Meteor. Soc.*, **98**, 45–68, <https://doi.org/10.1175/BAMS-D-15-00073.1>.
- Parker, M. D., and J. M. L. Dahl, 2015: Production of near-surface vertical vorticity by idealized downdrafts. *Mon. Wea.*

- Rev.*, **143**, 2795–2816, <https://doi.org/10.1175/MWR-D-14-00310.1>.
- Pazmany, A. L., J. B. Mead, H. B. Bluestein, J. C. Snyder, and J. B. Houser, 2013: A mobile rapid-scanning X-band polarimetric (RaXPo) Doppler radar system. *J. Atmos. Oceanic Technol.*, **30**, 1398–1413, <https://doi.org/10.1175/JTECH-D-12-00166.1>.
- Roberts, R. D., and J. W. Wilson, 1995: The genesis of three non-supercell tornadoes observed with Doppler radar. *Mon. Wea. Rev.*, **123**, 3436–6408, [https://doi.org/10.1175/1520-0493\(1995\)123<3408:TGOTNT>2.0.CO;2](https://doi.org/10.1175/1520-0493(1995)123<3408:TGOTNT>2.0.CO;2).
- Rotunno, R., 1977: Numerical simulation of a laboratory vortex. *J. Atmos. Sci.*, **34**, 1942–1956, [https://doi.org/10.1175/1520-0469\(1977\)034<1942:NSOALV>2.0.CO;2](https://doi.org/10.1175/1520-0469(1977)034<1942:NSOALV>2.0.CO;2).
- , 1986: Tornadoes and tornadogenesis. *Mesoscale Meteorology and Forecasting*, P. S. Ray, Ed., Amer. Meteor. Soc., 414–436.
- Ryzhkov, A. V., T. J. Schuur, D. W. Burgess, and D. S. Zrnić, 2005: Polarimetric tornado detection. *J. Appl. Meteor.*, **44**, 557–570, <https://doi.org/10.1175/JAM2235.1>.
- Schaefer, J. T., and R. Edwards, 1999: The SPC tornado/severe thunderstorm database. Preprints, *11th Conf. on Applied Climatology*, Dallas, TX, Amer. Meteor. Soc., 603–606.
- Schenkman, A. D., M. Xue, and M. Hu, 2014: Tornadogenesis in a high-resolution simulation of the 8 May 2003 Oklahoma City supercell. *J. Atmos. Sci.*, **71**, 130–154, <https://doi.org/10.1175/JAS-D-13-073.1>.
- Smith, R. K., and L. M. Leslie, 1978: Tornadogenesis. *Quart. J. Roy. Meteor. Soc.*, **105**, 107–127, <https://doi.org/10.1002/qj.49710544308>.
- , and —, 1979: A numerical study of tornadogenesis in a rotating thunderstorm. *Quart. J. Roy. Meteor. Soc.*, **104**, 189–199, <https://doi.org/10.1002/qj.49710443914>.
- Snyder, J. C., and H. B. Bluestein, 2014: Some considerations for the use of high-resolution mobile radar data in tornado intensity determination. *Wea. Forecasting*, **29**, 799–827, <https://doi.org/10.1175/WAF-D-14-00026.1>.
- , and A. V. Ryzhkov, 2015: Automated detection of polarimetric tornadic debris signatures using a hydrometeor classification algorithm. *J. Appl. Meteor. Climatol.*, **54**, 1861–1870, <https://doi.org/10.1175/JAMC-D-15-0138.1>.
- Storm Prediction Center, 2020: ONETOR: SPC National Severe Weather Database Browser (SeverePlot 3.0). Accessed October 2020, <https://www.spc.noaa.gov/climo/online/sp3/plot.php>.
- Tanamachi, R. L., H. B. Bluestein, J. B. Houser, S. J. Frasier, and K. M. Hardwick, 2012: Mobile, X-band polarimetric Doppler radar observations of the 4 May 2007 Greensburg, Kansas, tornadic supercell. *Mon. Wea. Rev.*, **140**, 2103–2125, <https://doi.org/10.1175/MWR-D-11-00142.1>.
- , —, M. Xue, W. Lee, K. Orzel, S. J. Frasier, and R. M. Wakimoto, 2013: Near-surface vortex structure in a tornado and in a sub-tornado-strength convective-storm vortex observed by a mobile, W-band radar during VORTEX2. *Mon. Wea. Rev.*, **141**, 3661–3690, <https://doi.org/10.1175/MWR-D-12-00331.1>.
- Thiem, K. J., 2016: Rapid-scan, polarimetric, mobile, Doppler-radar observations of the formation, evolution, and structure of the El Reno tornado of 31 May 2013. M.S. thesis, School of Meteorology, University of Oklahoma, 120 pp., <https://hdl.handle.net/11244/45410>.
- Trapp, R. J., and E. D. Mitchell, 1995: Characteristics of tornadic vortex signatures detected by WSR-88D radars. Preprints, *27th Conf. on Radar Meteorology*, Vail, CO, Amer. Meteor. Soc., 517–518.
- , and R. Davies-Jones, 1997: Tornadogenesis with and without a dynamic pipe effect. *J. Atmos. Sci.*, **54**, 113–133, [https://doi.org/10.1175/1520-0469\(1997\)054<0113:TWAWAD>2.0.CO;2](https://doi.org/10.1175/1520-0469(1997)054<0113:TWAWAD>2.0.CO;2).
- , E. D. Mitchell, G. A. Tipton, D. W. Effertz, A. I. Watson, D. L. Andra Jr., and M. A. Magsig, 1999: Descending and nondescending tornadic vortex signatures detected by WSR-88Ds. *Wea. Forecasting*, **14**, 625–639, [https://doi.org/10.1175/1520-0434\(1999\)014<0625:DANTVS>2.0.CO;2](https://doi.org/10.1175/1520-0434(1999)014<0625:DANTVS>2.0.CO;2).
- Vasiloff, S. V., 1993: Single-Doppler radar study of a variety of tornado types. *The Tornado: Its Structure, Dynamics, Prediction, and Hazards, Geophys. Monogr.*, Vol. 79, Amer. Geophys. Union, 223–231.
- Wakimoto, R. M., and J. W. Wilson, 1989: Non-supercell tornadoes. *Mon. Wea. Rev.*, **117**, 1113–1140, [https://doi.org/10.1175/1520-0493\(1989\)117<1113:NST>2.0.CO;2](https://doi.org/10.1175/1520-0493(1989)117<1113:NST>2.0.CO;2).
- , C. Liu, and H. Cai, 1998: The Garden City, Kansas, storm during VORTEX 95. Part I: Overview of the storm's life cycle and mesocyclogenesis. *Mon. Wea. Rev.*, **126**, 372–392, [https://doi.org/10.1175/1520-0493\(1998\)126<0372:TGCKSD>2.0.CO;2](https://doi.org/10.1175/1520-0493(1998)126<0372:TGCKSD>2.0.CO;2).
- Wang, A., Y. Pan, and P. M. Markowski, 2020: The influence of turbulence memory on idealized tornado simulations. *Mon. Wea. Rev.*, **148**, 4875–4892, <https://doi.org/10.1175/MWR-D-20-0031.1>.
- Wicker, L. J., and R. B. Wilhelmson, 1995: Simulation and analysis of tornado development and decay within a three-dimensional supercell thunderstorm. *J. Atmos. Sci.*, **52**, 2675–2703, [https://doi.org/10.1175/1520-0469\(1995\)052<2675:SAOTD>2.0.CO;2](https://doi.org/10.1175/1520-0469(1995)052<2675:SAOTD>2.0.CO;2).
- Wienhoff, Z. B., H. B. Bluestein, D. W. Reif, R. M. Wakimoto, L. J. Wicker, and J. M. Kurdzo, 2020: Analysis of debris signature characteristics and evolution in the 24 May 2016 Dodge City, Kansas, tornadoes. *Mon. Wea. Rev.*, **148**, 5063–5086, <https://doi.org/10.1175/MWR-D-20-0162.1>.
- Wilczak, J. M., D. E. Wolfe, R. J. Zamora, B. Stankov, and T. W. Christian, 1992: Observations of a Colorado tornado. Part I: Mesoscale environment and tornadogenesis. *Mon. Wea. Rev.*, **120**, 497–521, [https://doi.org/10.1175/1520-0493\(1992\)120<0497:OOACTP>2.0.CO;2](https://doi.org/10.1175/1520-0493(1992)120<0497:OOACTP>2.0.CO;2).
- Wurman, J., and M. Randall, 2001: An inexpensive, mobile, rapid-scan radar. Preprints, *30th Conf. on Radar Meteorology*, Munich, Germany, Amer. Meteor. Soc., 98–100.
- , and K. Kosiba, 2013: Finescale radar observations of tornado and mesocyclone structures. *Wea. Forecasting*, **28**, 1157–1174, <https://doi.org/10.1175/WAF-D-12-00127.1>.
- , —, P. Markowski, Y. Richardson, D. Dowell, and P. Robinson, 2010: Finescale single- and dual-Doppler analysis of tornado intensification, maintenance, and dissipation in the Orleans, Nebraska, supercell. *Mon. Wea. Rev.*, **138**, 4439–4455, <https://doi.org/10.1175/2010MWR3330.1>.
- Xue, M., D.-H. Wang, J.-D. Gao, K. Brewster, and K. K. Droegemeier, 2003: The Advanced Regional Prediction System (ARPS), storm-scale numerical weather prediction and data assimilation. *Meteor. Atmos. Phys.*, **82**, 139–170, <https://doi.org/10.1007/s00703-001-0595-6>.

- , M. Hu, and A. D. Schenkman, 2014: Numerical prediction of the 8 May 2003 Oklahoma City tornadic supercell and embedded tornado using ARPS with the assimilation of WSR-88D data. *Wea. Forecasting*, **29**, 39–62, <https://doi.org/10.1175/WAF-D-13-00029.1>.
- Yokota, S., J. Miino, H. Seko, M. Kunii, and H. Yamauchi, 2018: Important factors of tornadogenesis as revealed by high-resolution ensemble forecasts of the Tsukuba supercell tornado of 6 May 2012 in Japan. *Mon. Wea. Rev.*, **146**, 1109–1132, <https://doi.org/10.1175/MWR-D-17-0254.1>.
- Ziegler, C. L., E. N. Rasmussen, T. R. Shepherd, A. I. Watson, and J. M. Straka, 2001: The evolution of low-level rotation in the 29 May 1994 Newcastle–Graham, Texas, storm complex during VORTEX. *Mon. Wea. Rev.*, **129**, 1339–1368, [https://doi.org/10.1175/1520-0493\(2001\)129<1339:TEOLLR>2.0.CO;2](https://doi.org/10.1175/1520-0493(2001)129<1339:TEOLLR>2.0.CO;2).